

# SANDIA REPORT

SAND96-2329 • UC-906

Unlimited Release

Printed February 1997

## Laboratory Directed Research and Development Final Report Intelligent Tools for On-Machine Acceptance of Precision Machined Components

Naomi G. Christensen, Lane D. Harwell, Andrew Hazelton

Prepared by  
Sandia National Laboratories  
Albuquerque, New Mexico 87185 and Livermore, California 94550  
for the United States Department of Energy  
under Contract DE-AC04-94AL85000

Approved for public release; distribution is unlimited.

Issued by Sandia National Laboratories, operated for the United States Department of Energy by Sandia Corporation.

**NOTICE:** This report was prepared as an account of work sponsored by an agency of the United States Government. Neither the United States Government nor any agency thereof, nor any of their employees, nor any of their contractors, subcontractors, or their employees, makes any warranty, express or implied, or assumes any legal liability or responsibility for the accuracy, completeness, or usefulness of any information, apparatus, product, or process disclosed, or represents that its use would not infringe privately owned rights. Reference herein to any specific commercial product, process, or service by trade name, trademark, manufacturer, or otherwise, does not necessarily constitute or imply its endorsement, recommendation, or favoring by the United States Government, any agency thereof, or any of their contractors or subcontractors. The views and opinions expressed herein do not necessarily state or reflect those of the United States Government, any agency thereof, or any of their contractors.

Printed in the United States of America. This report has been reproduced directly from the best available copy.

Available to DOE and DOE contractors from  
Office of Scientific and Technical Information  
P.O. Box 62  
Oak Ridge, TN 37831

Prices available from (615) 576-8401, FTS 626-8401

Available to the public from  
National Technical Information Service  
U.S. Department of Commerce  
5285 Port Royal Rd  
Springfield, VA 22161

NTIS price codes  
Printed copy: A04  
Microfiche copy: A01

SAND96-2329  
Unlimited Release  
Printed February 1997

Distribution  
Category UC-906

## Laboratory Directed Research and Development

### Final Report

# Intelligent Tools for On-Machine Acceptance of Precision Machined Components

Naomi G. Christensen  
Precision Mechanical Products Department

Lane D. Harwell  
Mechanical Process Engineering Department

Andrew Hazelton  
Advanced Manufacturing Technologies for Metals Processing Department

Sandia National Laboratories  
P. O. Box 5800  
Albuquerque, NM 87185-0319

### Abstract

On-Machine Acceptance (OMA) is an agile manufacturing concept being developed for machine tools at SNL. The concept behind OMA is the integration of product design, fabrication, and qualification processes by using the machining center as a fabrication and inspection tool. This report documents the final results of a Laboratory Directed Research and Development effort to qualify OMA.

### **Acknowledgments**

Thanks to Don Sheaffer, Department 8120, Mark Powell, Department 9611, and Marcey Abate, Department 12323, for their contributions to this final report. Thanks to Tony Bryce, and Dennis Clingan, Department 1484, Phil Skogmo, Department 2645, and Charles Steinhaus, Department 8240, for their assistance in writing this report.

## Contents

1.0	Introduction .....	5
1.1	Benefits of OMA .....	6
1.2	Issues of OMA.....	7
2.0	Scope .....	7
3.0	Acronyms and Definitions .....	8
4.0	Facilities, Equipment, Hardware/Software, Standards, and Methods	9
4.1	SNL/NM Summary.....	9
4.2	SNL/CA Summary .....	9
5.0	Benchmarking Activities.....	10
5.1	SNL/CA Market Survey Summary .....	10
5.2	Literature Search Keywords .....	12
6.0	Artifact Definition Summary .....	14
6.1	SNL/NM Artifact Definition Summary .....	14
6.2	SNL/CA Artifact Definition Summary .....	14
7.0	SNL/NM Design of Experiment Summary .....	16
7.1	Data Acquisition Summary .....	16
7.2	Inspection Plan Summary .....	17
7.3	Probe Parameter Summary .....	18
7.4	Milling Machine Parameter Summary .....	18
8.0	SNL/CA Design of Experiment Summary.....	19
8.1	Phase One Summary .....	19
8.1.1	Phase One Benchmark Study.....	19
8.1.2	Phase One Error-Correction Study .....	20
8.2	Phase Two Summary .....	22
8.2.1	Graphic Visualization of Sensor Data .....	23
9.0	OMA Time and Cost Analysis.....	23
10.0	SNL/NM Data Analysis.....	24
10.1	Thermal Data Analysis and Summary .....	25
10.2	Machine Error .....	28
10.2.1	Machine Error Analysis.....	29
10.2.2	Machine Error Analysis Summary .....	31
10.3	Statistical Data Analysis .....	32
10.3.1	F-Test and Paired T-Test Summary .....	33

10.4	Uncorrected and Corrected Data Analysis .....	35
10.4.1	Accuracy Analysis .....	36
10.4.2	Repeatability Analysis .....	40
10.5	Accuracy and Repeatability Analysis Summary .....	46
11.0	SNL/CA Data Analysis .....	46
11.1	Phase One Analysis .....	47
11.1.1	Benchmark Analysis .....	47
11.1.2	Error-Corrected Analysis .....	52
11.1.3	Phase One Analysis Summary .....	58
11.2	Phase Two Graphic Visualization Demonstration .....	59
12.0	SNL/NM OMA Issues .....	61
12.1	Probing Strategies .....	61
12.2	Probe (Sensor) Technologies .....	61
12.3	Part Location on Machine .....	62
12.4	Probe Alignment and Probe to Part Coordinate System .....	62
12.5	Data Mismatch .....	62
12.6	Approach/Retract Speed Variation .....	63
12.7	QUALSTAR .....	64
13.0	Future OMA Activities .....	62
13.1	OMA Activities at Allied-Signal, FM&T .....	62
13.2	OMA Contacts .....	63
13.3	Further Development of OMA .....	64
14.0	Figures and Tables .....	66
15.0	References .....	67

## 1.0 Introduction

On-Machine Acceptance (OMA) is an agile manufacturing concept for machine tools being developed at Sandia National Laboratories (SNL). OMA was pursued as a two-year Laboratory Directed Research and Development (LDRD) project whose goal was to integrate the design, manufacturing, and product qualification activities and apply the hardware/software and principles to accept machined product directly off the machine tool.

The highlighted modules or activities illustrated in Figure 1. are those eliminated by using the OMA approach to product acceptance for milling centers.

The two year LDRD allowed us to demonstrate a proof-of-concept that OMA technologies will allow us to make parts better, faster, and cheaper by ensuring that turned and milled parts meet acceptance requirements before removal from the machine tool. Our original scope of work was far too great to address problems such as probing strategy, on-machine deburring, etc., given the funding and time considerations. We chose instead, to concentrate resources on data analysis and proof-of-concept and try to address these other issues via cooperative efforts with industry partners or partners within the Nuclear Weapons Complex (NWC).

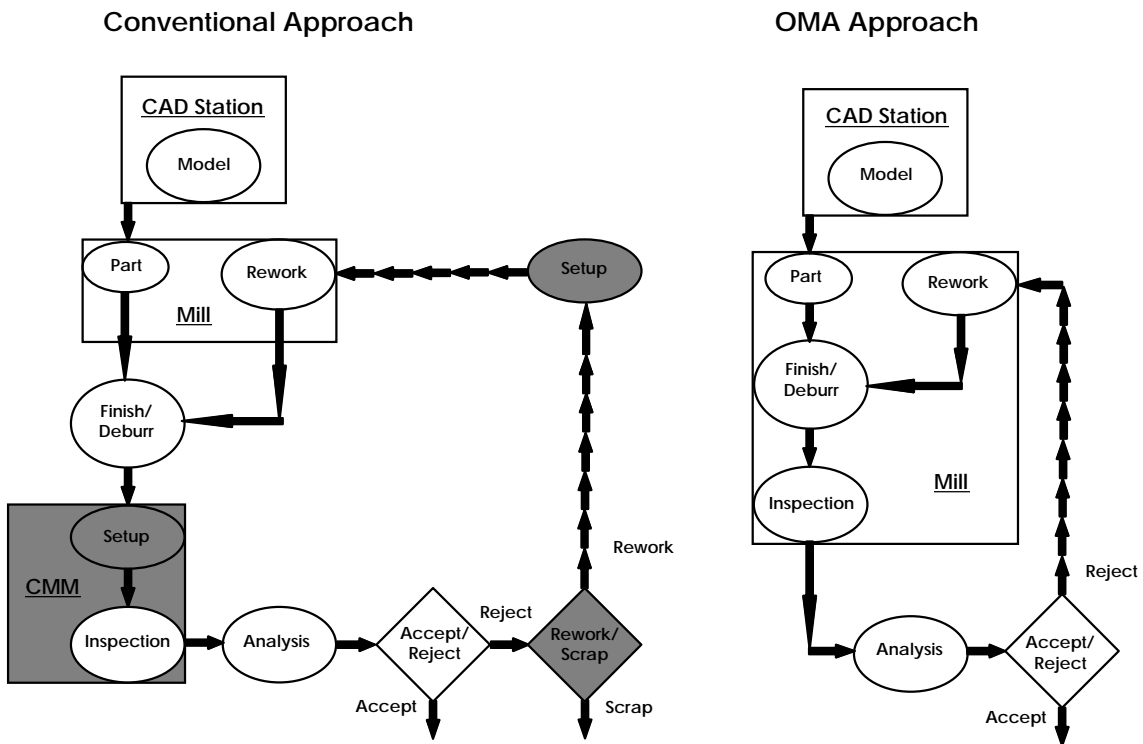


**Figure 1. - Comparison of Conventional Product Realization to OMA**

## 1.1 Benefits of OMA

The benefits realized by implementing OMA are many. The first of these benefits is the change from a reactive inspection environment to a proactive control environment where the machining process and the machine are well understood. Data collected during machining can be used to monitor, characterize, and ultimately control the process. Proactive control is brought about by a better understanding of the process variables, the magnitude of their effect on the process, and the controls that minimize their effect.

A controlled and understood process produces a reliable, quality product because the process and machine have been characterized and qualified. Inspection after the product comes off the machine tool is not a cost-effective or proactive means to identify nonconforming product. Consider that a nonconforming part may be machined and awaiting inspection while the machine continues to produce nonconforming product. When the nonconformances are finally discovered, either the whole lot is rejected, or all the parts must be inspected and the data analyzed to weed out salvageable parts. The loss of resources, the time spent machining, inspecting, and reworking, the materials, and loss of schedule all contribute to the cost of the product. Focusing resources to monitor, adjust, and control the machining process before the part is removed from the machine tool is preferable to identifying nonconforming product after-the-fact.

A second benefit of OMA is the elimination of non-value-added activities from the process. Consider the design, fabrication, and maintenance of hard gages - gages that are not flexible to design change and require long lead times to manufacture. These gages cost money to fabricate and maintain and also add to the cost of the product. Inspection on a CMM (Coordinate Measuring Machine) or other inspection equipment may also require new inspection fixtures that add to the product cost.

Reworking a nonconforming part is a nonvalue-added activity because it increases the cost of the product without adding to its value. Because the part is removed from the machine tool for inspection, the part coordinate system needs to be reestablished manually on the machine tool for rework. In contrast, inspection on the machine tool is more efficient than inspection on the CMM because the part coordinate system is intact if the part needs rework and there is material to remove.

Once the part is removed from its fixture, its geometry usually distorts to a free-state condition that is different from the fixtured condition. Part

distortion may cause rejection or scrapping of product that was actually in conformance before removal from the machining fixture or installation into an inspection fixture. Inspection on the machine will provide valuable information regarding the part condition prior to any secondary inspection and the distortion that occurs as a result.

If the part meets design specifications, it can be accepted directly off the machine tool. If the part does not conform, the inspection information can be input back to the machine tool for necessary corrections without disturbing the part setup.

A third benefit is increased agility of the machining process. Redirecting resources to value-added activities and real-time data analysis serve to make a process more agile and shorten the product cycle time. Integration of the design, manufacturing, and qualification activities is accomplished by using the electronic part model to drive all three of these product realization activities resulting in a rapid response to design changes and changing process parameters. Using sensors to gather data during processing allows the process to be evaluated and adjusted to control part geometry and tolerances. Using a "soft gage" to analyze the part data in real time allows disposition of the product almost immediately.

## **1.2 Issues of OMA**

Along with the benefits realized from implementing OMA are several issues that need to be addressed. The biggest issue that needs to be addressed is the fact that OMA requires a major change in the philosophy of product acceptance. Resistance to change the current philosophy results in arguments such as "The independence of inspection is not preserved -- that's like letting a fox loose in the henhouse.", or "Using a machine tool for inspection isn't efficient use of the machine -- it should be cutting chips.", or "The machine won't be able to detect errors in the part because it will make measurements with the same errors it that it built into the part." Other issues that must be addressed are lack of knowledge of the machine and machining process, including the effect of temperature on the part measurements. Furthermore, there are issues common to both OMA and CMM inspections -- issues such as probe error, probing strategy, and data interpretation that need to be addressed.

## **2.0 Scope**

This report covers SNL/NM OMA development performed from December 1995 to September 1996. Detailed information regarding the SNL/NM OMA software and hardware, design of experiment, probe parameters, probe paths, inspection strategies, and data analysis, done from October 1994 to November 1995 is documented in SAND95-3061, "Laboratory Directed Research and Development - Interim Report - Intelligent Tools for

On-Machine Acceptance of Precision Machined Components”, authors, N. G. Christensen, L. D. Harwell, and M. L. Abate. <sup>1</sup>

This report also contains detailed information about the SNL/CA OMA development effort, software and hardware, design of experiment, probe parameters, probe paths, inspection strategies, and data analysis performed from October 1994 to September 1996. Furthermore, this final report on the LDRD may contain minor data, transcription, or analysis errors of which we are not aware.

### 3.0 Acronyms and Definitions

ANOVA	Analysis of Variance.
ASME	American Society of Mechanical Engineers.
ANSI	American National Standard Institute.
AS-FM&T	Allied-Signal, Federal Manufacturing and Technology
CAA	Computer-Aided Accuracy.
CAD	Computer-Aided Design.
CAM-I	Consortium for Advanced Manufacturing International.
CMM	Coordinate Measuring Machine.
CNC	Computer Numerical Control.
DMIS	Dimensional Measuring Interface Standard.
DP	Defense Programs.
GTS	Gas Transfer System.
IGES	International Graphics Exchange Standard.
IMTL	Integrated Manufacturing Technologies Laboratory.
MMI	Markowitz and McNaughton, Inc..
NWC	Nuclear Weapons Complex. As of this writing, the reconfigured NWC consists of design agencies, Los Alamos National Laboratory, Lawrence Livermore National Laboratory, Sandia National Laboratories, and the production agencies, Allied-Signal, Federal Manufacturing and Technology, and Mason-Hanger Pantex Plant.
OMA	On-Machine Acceptance.
OMI	On-Machine Inspection. The difference between OMA and OMI is that inspection on a machine tool does not necessarily guarantee acceptance of the machined product. The data obtained by the inspection must be analyzed to determine if the part meets the design requirement before it can be accepted.
OMFA	On-Machine Finishing and Acceptance. The difference between OMA and OMFA is that the part is finished and deburred while on the machine tool with its coordinate

system intact. The part is then probed, the data analyzed and the part accepted.

PCM	Process Characterization Methodology.
PDP	Process Development Program.
SNL/NM	Sandia National Laboratories, New Mexico.
SNL/CA	Sandia National Laboratories, California.
VRML	Virtual Reality Modeling Language.
WR	War Reserve.

## **4.0 Facilities, Equipment, Hardware/Software, Standards, and Methods**

This section documents the equipment, hardware, software, standards, methods, and approaches used to perform LDRD work at both the SNL/NM and SNL/CA sites.

### **4.1 SNL/NM Summary**

The equipment used to perform LDRD work at SNL/NM included a Computer Numerical Control (CNC) Boston Digital BostoMatic 300, 4-axis milling machine with probing capability and a resolution of 0.00002". The functional envelope of the BostoMatic is 18.0" X 12.0" X 12.0" for the X, Y, and Z axes respectively. A Renishaw TP1-S touch trigger probe was used to probe the parts fabricated on the machine.

A CNC Zeiss UPMC 550 Computer-Aided Accuracy (CAA) CMM was used as the standard by which to compare milling machine data. The Zeiss has a resolution of 0.2  $\mu\text{m}$  (~0.000008") with a functional envelope of the Zeiss is 550 mm X 500 mm X 500 mm (~21.5" X 20.5" X 20.5") for the X, Y, and Z axes respectively. A Zeiss Universal Three-Dimensional probe head was used to probe the part.

The software used for the LDRD work was the same as documented in the interim report with one exception.<sup>1</sup> The exception was the addition of Silma for program probing paths for both the BostoMatic and Zeiss using a ProEngineer artifact model. Silma generates a Dimensional Measuring Interface Standard (DMIS) file per the American National Standard Institute/Consortium for Advanced Manufacturing-International (ANSI/CAM-I)101-1990 specification which we translated into a Zeiss probing path via UMESS and the Version 2.7 Zeiss DMIS translator.

The general method employed to qualify OMA was to machine and measure hardware on the BostoMatic, measure the same hardware at the same locations on the Zeiss, and compare the measurements from both machines to determine the pure measurement capability of the BostoMatic.

### **4.2 SNL/CA Summary**

Two distinct approaches were used at SNL/CA to advance OMA technology. Phase one of the LDRD study used machine kinematics characterization combined with on-machine probing to perform

dimensional analysis and verify part geometry. A benchmark study was performed to better understand and quantify systematic errors between on-machine inspections and independent inspections.

A second study conducted during phase one implemented limited error correction to determine the accuracy of on-machine inspections versus independent (off-machine) inspections. The equipment used to perform phase one LDRD work was a LeBlond Baron 25 CNC lathe with a Fanuc controller. Inspection of an artifact resembling a Gas Transfer System (GTS) was performed on the LeBlond outfitted with a Renishaw touch trigger probe as well as a CNC Moore CMM. The inspection data was output as diameter, Z position, and theta to a PC running Geomet inspection software. The data was further analyzed using Microsoft Excel.

Phase two of the LDRD study coupled in-process sensing and visualization of sensor data linked directly to the design specifications. The emphasis of phase two was to demonstrate feasibility of an easily interpreted, three dimensional, graphical visualization system to allow a more complete understanding of the process and manufacturing defects. The equipment used to perform phase two LDRD work was a Haas Mill. Data acquired by the Haas mill was transformed and color-mapped onto a ProEngineer part model. The machining process was monitored using three-dimensional tool force, vibration, acoustic emissions, and torque sensors.

## **5.0 Benchmarking Activities**

This section documents the results of benchmarking activities which include a market survey and a literature search conducted at the SNL/NM and SNL/CA sites.

### **5.1 SNL/CA Market Survey Summary**

A market survey was contracted to Markowitz and McNaughton, Inc. (MMI) by SNL/CA at the end of 1995 to determine the interest of manufacturers of machined hardware in OMA technology. MMI produced a report entitled "Status of On-Machine Acceptance Systems and Methodologies in Small Lot, High Precision Machining Applications", which summarized survey data from a total of ten manufacturers/end users and two probe manufacturers. <sup>2</sup>

The primary objectives of this study were to:

- Identify and understand the tools and methodologies used in the acceptance of small lot, high precision machined parts,
- Identify and compare the manufacturers and products of machines and tools used in the measurement and acceptance of high precision machined parts,
- Understand how end-users test/measure precision machined parts for acceptable conformance to design specifications and define the disposition procedure for parts found to be outside of acceptable specifications,
- Determine awareness of OMA technologies and methodologies,
- Determine the decision making process for new testing/analytical systems, including the primary purchase decision criteria,
- Identify existing or development stage technologies in OMA,
- Identify an acceptable price range for a software-based OMA technology, and
- Characterize the market for small lot, high precision machined parts,
- Characterize the end-user. <sup>2</sup>

Figure 2. illustrates the relative interest of these manufacturers in OMA. MMI noted that generally, the most interest in OMA came from aerospace and defense industries, followed by the nuclear, medical, and machinery/tooling industries because these industries are highly regulated, have small lots, and high cost products with high precision requirements. The industries having the least interest in OMA were the automotive and consumer goods industries that have high production volumes with a limited need for high precision. <sup>2</sup>

The report also contained detailed information perceived potential problems or concerns of these end users:

- Machine tool accuracy and positioning capability,
- Isolation and elimination of systematic machine tool error,
- Probe accuracy,
- Protection of probe assembly from coolant, chips, etc.,
- Development of interface between probe and CNC machine,
- Thorough software-based analysis of measurement data and overall machining process,
- Off-line programming required by machine operator, particularly when initiating a new parts program,
- Integration of OMA module into a total measuring system,
- Cost,

- Potential for lost spindle time (machine down time) due to inspection, and
- Potential for loss of both cutting (production) and inspection capabilities if system were to break down. <sup>2</sup>

We have recognized and have attempted to address the concerns and problems listed above in the course of this LDRD. Furthermore, MMI recommended that SNL establish direct contact with the end-users expressing an interest in learning more about OMA to collaborate with SNL in its development. This contact should help Sandia gain a clearer understanding of the development status of potentially competing OMA technologies, or opportunities to partner with these industries to leverage resources for OMA development. <sup>2</sup>

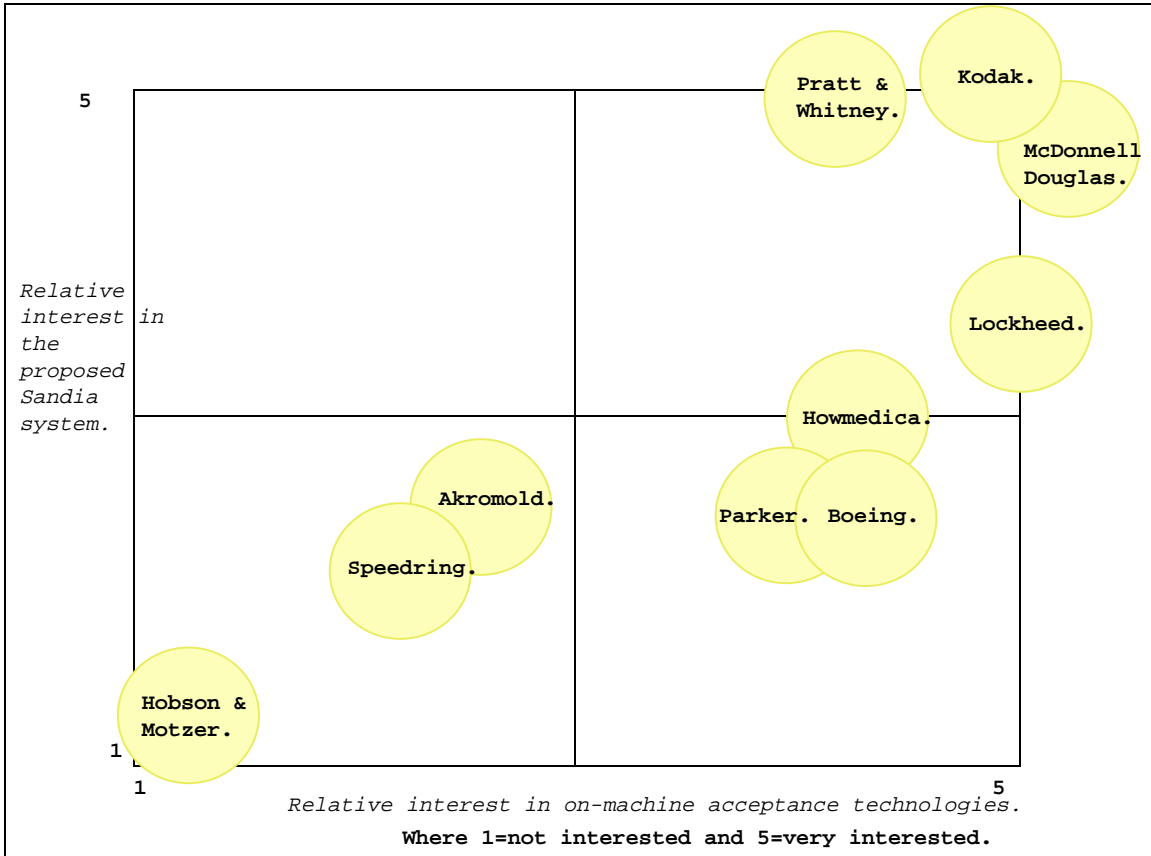


Figure 2. - Relative Interest in OMA of Potential End Users

## 5.2 Literature Search Keywords

A third literature search was conducted in January, 1996 to update information on On-Machine Inspection (OMI) and OMA to determine the status of any work falling within the LDRD scope being done in industry. This literature search yielded several new articles which are included in SAND96-8237, "Bibliography of Papers, Reports, and Presentations Related to Point-Sample Dimensional Measurement Methods for Machined Part Evaluation", authored by J. M. Baldwin. <sup>3</sup>

**Keywords for OMA Literature Search (1-26-96)**

Machine error

Coordinate Measuring Machine (CMM) measurement error

Measurement error

Measurement uncertainty

Positioning error

Error modeling

Error simulation

Error prediction

Error compensation

Statistical error prediction

Machine tool positioning error

ANSI/ASME B5.54

Positioning error

Error modeling

Error simulation

Error prediction

Error compensation

Statistical error prediction

Error simulation

Monte Carlo simulation

Error prediction

Error modeling

Statistical error prediction

Measurement error

Error simulation

Monte Carlo simulation

Error prediction

Statistical error prediction

Error modeling

Positioning error

Error simulation

Monte Carlo simulation

Error prediction

Statistical error prediction

Error modeling

Statistical error prediction

Monte Carlo simulation

## Statistical error modeling

## 6.0 Artifact Definition Summary

This section documents the rationale for choosing artifacts, geometry, and tolerances to perform LDRD studies, analysis, and qualification of OMA at both the SNL/NM and SNL/CA sites.

### 6.1 SNL/NM Artifact Definition Summary

The SNL/NM artifact chosen for the LDRD resembled a nuclear weapon safety device called a stronglink that is used to prevent accidental arming or nuclear material release. The artifact was chosen for its size, tolerances, and complex geometry. The artifact was modeled in both ProEngineer and ANVIL-5000 with slight changes to incorporate certain features into the LDRD artifact that we wished to measure. The material chosen for the LDRD artifact was 6061 aluminum to minimize tool wear.

The LDRD artifact was created from a disk-shaped blank that was machined on a lathe. The primary datum, -A- is a plane on the top surface of the artifact used to establish spatial orientation or a plane normal to the Z axis. The secondary datum, -B-, is a hole in the center of the artifact used to establish the origin of the coordinate system. Datum -C- is a vertical plane running parallel to the Y-axis that is used to orient the artifact to the X and Y axes of the coordinate system. Figure 3. illustrates the SNL/NM artifact and the location of probed points.

### 6.2 SNL/CA Artifact Definition Summary

The phase one SNL/CA artifact was chosen to reasonably represent a generic reservoir for a nuclear weapon GTS (Figure 4.). Because the standard GTS components were considered too difficult to machine inexpensively, a simpler reservoir artifact was designed with the following features:

- A J-groove diameter for fixture simplicity,
- Accessible datum surfaces for ease of analysis and probe assisted part setup,
- An undercut surface for probing in the +Z direction,
- A face groove for probing in the +X direction,
- Multiple form tolerances,
- Simplified geometry for ease of machining, and
- Easily machined 303 stainless steel material.

These features combined to make an artifact that is relatively inexpensive to machine yet contains a wealth of features for geometric analysis and comparison. Bar stock was first machined as cone shaped parts on a separate machine to prepare the artifacts for further processing.



Figure 3. - SNL/NM OMA Artifact and Probe Point Location

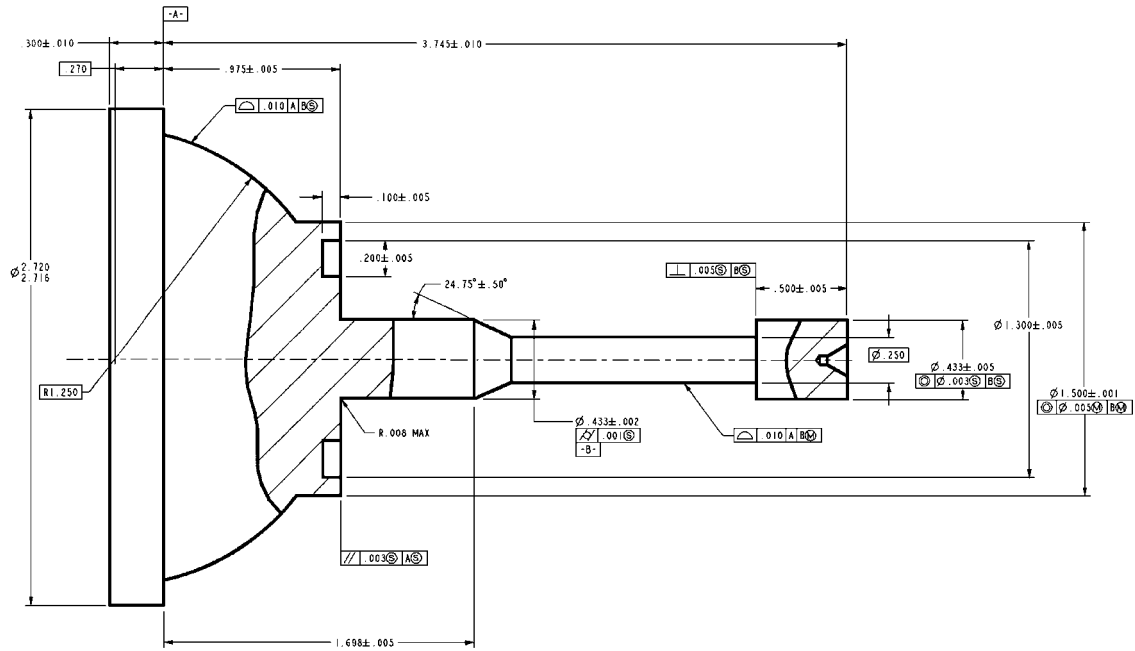


Figure 4. - SNL/CA OMA Artifact

The phase two artifact was a rectangular block with several counterbored holes. Sensor data acquired during machining of the block was superimposed over a ProEngineer model of the artifact.

## **7.0 SNL/NM Design of Experiment Summary**

This section documents the design of experiment rationale for performing LDRD studies, analysis, and qualification of OMA at the SNL/NM site.

### **7.1. Data Acquisition Summary**

Sources of error that could affect data acquisition were controlled and documented as thoroughly as possible during machining and inspection to ensure that the data acquired on either machine were not affected. Variation of equipment parameters, data gathering procedures, human intervention, etc., could make the data impossible to compare so we placed strict controls on the processes to allow us to distinguish error sources and attribute causes to data anomalies detected during data analysis. Worksheets were used to record information on machine and probe settings, file names, processing times, and unusual occurrences during the machining and/or measurement processes.

The number of artifacts chosen for the final run was seven. The plan for measuring the artifacts required five measurement runs on all of these artifacts with both machines. The seventh artifact would have an additional five measurement runs performed on it with the probe head being removed and repositioned prior to each measurement to determine the repeatability of this action. This measurement plan resulted in forty data files for the BostoMatic and thirty-five files for the Zeiss. Each artifact was marked sequentially as it came off the BostoMatic to record the process sequence.

The probing path for both BostoMatic and Zeiss was generated on Silma and virtually crash-tested on a ProEngineer model of the artifact. A DMIS file was downloaded from Silma as two identical probing paths for both machines. Duplicating the probing paths allowed us to compare the two data sets point-for-point and determine raw X, Y, and Z measurement capability of the BostoMatic. The number of probed points on each artifact was clearly defined and controlled on the artifact geometries by the DMIS probe path. For the most part, the Zeiss served as the measurement standard or master gage to which the BostoMatic measurements were compared.

Data was collected in metric units to allow us to collect data accurate to four significant digits. Three digits in metric units (0.001 mm) could be translated to 0.000040" (five significant English decimal places) which was one more significant digit than collected in our previous OMA studies.

Although we had also planned to construct geometry using the discrete data points, time and budget constraints prevented this further analysis. We recommend that future analysis of data acquired in other studies similar to this include the analysis of constructed geometry. Analyzing constructed geometry from both machines using the same measurement software should allow a comparison of measurement capability for feature size and location; although, if the X, Y, and Z locations are similar, the feature size and location should also be similar.

## 7.2 Inspection Plan Summary

The artifact inspection plan was designed to control the number and location of data points on various artifact geometries. Thus, the artifact was probed at eight co-planar points located 45° apart points on circles, at least three points on planes, two points on radial or straight slots, and sixteen points on cylinders for a total of 145 points. The Silma-generated probe path provided better control of probing direction and crash detection for both the BostoMatic and Zeiss.

The probe direction was typically defined by a vector in the X, Y, and Z axes. No three component probing vectors were probed on the artifacts. Factors such as surface finish, method of fabrication, deviations in geometric form, or feature size that influence probe point density or location were not considered when planning the artifact probing paths

A known spherical artifact of 22.225 mm (0.875") was probed prior to each measurement run. The sphere measurement served three purposes. First, suspected problems on either machine (probe error or machine crashes) could be verified immediately by evaluating measurements of the standard. Second, measuring an artifact of known size added consistency from part to part during the machining process and allowed us to detect changes in the measurements due to thermal expansion, tool wear, or other process factors. Third, probing the standard allowed us to compare the pure measurement capability of the BostoMatic to a precision measuring device (the Zeiss) without any bias introduced by geometric imperfections of the BostoMatic.

An optimal probing strategy (data density, probe point location, etc.) was not pursued because of time and budget constraints. We believe that other organizations such as CAM-I will develop a protocol for probing strategies based on the methods of fabrication. The CAM-I initiative will serve as a basis for probing machined product on both machine tools and CMMs. The clear and concise mathematical definitions for planes, circles, etc. contained in ANSI Y14.5M Tolerancing and Dimensioning standard should also provide insight for developing probing strategies, resulting in consistent definition, interpretation, and measurement of various geometries.

### **7.3 Probe Parameter Summary**

Probe parameters including probing speeds, stylus diameters, probing pressures, and probing direction were duplicated as much as possible on both machines to allow us to eliminate probe error from the measurements. Probe stylus diameters for both machines was 1.0 mm (0.0394") to minimize measurement error introduced by measurement software probe diameter corrections. Probing force settings were also duplicated between the two machines to 0.1 Newton ( $\text{kg} \cdot \text{m}/\text{sec}^2$ ). The Renishaw probe used for the BostoMatic differs mechanically from the Zeiss probe, but studies to determine the extent of the differences and their effect on the measurement data were not performed.

In the interim report, we noted that the BostoMatic data showed poor repeatability. Experiments performed to determine the cause of the repeatability problem identified the differences in probing direction between the Zeiss and the BostoMatic. The Zeiss takes data on the approach and the BostoMatic takes data on the retract, so we suspect that the data may be affected by overtravel. Any data analysis shown later in this report does not include error correction for, or isolation of, the potential errors caused by the differences in probing direction. Probing direction may be partially responsible for the difference in the measurements depicted in the QUALSTAR-corrected data (see Section 10.4.1).

### **7.4 Milling Machine Parameter Summary**

The BostoMatic machining parameters have a twofold impact on the artifact measurements. First, the machining parameters affect the artifact quality -- whether it meets tolerance requirements, its surface finish, and amount of deviation from true geometric form. The artifact quality in turn,

affects the ability to obtain accurate measurements. Machine tool parameters such as tool speeds, tool feed rate, depth of cut, and number of finish passes all impact part quality. Other related factors such as tool wear and tool "spring back" are dependent on the machine tool parameters, but they too, affect the artifact quality.

Second, the machine feed rate also controls the approach and retract speeds of the probe as it captures data points on the artifact. The effects of approach and retract speeds on overtravel of the probe and measurement accuracy are discussed in Section 7.3 above.

The spindle speed settings for the machining process ranged from a low of 5250 rpm to a high of 6650 rpm. The tool feed rates for the machining process ranged from a low of 2.5"/minute (~0.042" per second) to a high of 15.0"/minute (~0.233" per second). Different spindle speeds and feed rates were required because of the different tools used to machine the artifact.

## **8.0 SNL/CA Design of Experimental Summary**

This section documents the two-phase design of experiment rationale for performing LDRD studies, analysis, and qualification of OMA conducted at the SNL/CA site.

### **8.1. Phase One Summary**

Phase one was conducted in two parts. The phase one benchmark study was performed to better understand the similarities and differences between on-machine inspections and independent inspections. The phase one error correction study implemented limited error correction to determine the accuracy of on-machine inspections versus independent (off-machine) inspections. The two studies are detailed below.

#### **8.1.1 Phase One Benchmark Study**

A probing system was chosen to measure all GTS artifact features on the LeBlond CNC turning center for phase one study. Because lathe probes are not fitted with indexable heads, the task of probing features in four directions (-X for outer diameters, +X for inner diameters, -Z for front faces, and +Z for undercuts) required a special probe configuration with multiple styli. The small geometry of the GTS artifact forced the two probe tips to be closer than 5 mm, requiring us to consider a specially made probe stylus which was too expensive and complicated for the phase one study. As a result, we decided not to machine the artifact face groove or probe in the +X direction, so a Renishaw touch probe was used on the LeBlond lathe to collect data. The probe stylus chosen to measure the artifact was

a 1 mm diameter ruby tip mounted on a steel shank approximately 20 mm long. The probe was mounted with the stylus aligned along the X axis.

After discussion with a statistician, we decided that 12 artifacts would be sufficient to provide a statistically significant sample provided multiple, related features were measured on each part. In addition, to test repeatability of measurements, every fifth part was measured twice.

The prepared 303 stainless steel stock was loaded into lathe soft jaws and the tailstock applied to the stem end to secure it. After turning, the tailstock was retracted, the probe was positioned, and the artifact was probed. Inspection data was output as artifact diameter, Z axis data, and theta to Geomet software. Probe data was output in a data file as X, Y, and Z point data. After probing, the part was removed, another piece of prepared stock was inserted, and the process repeated.

The artifacts were then dimensionally inspected on a CMM; however, the CMM was limited in its ability to measure the part because it did not have a rotary table. Consequently, the CMM was not able to probe the same points taken on the machine tool, but each part was probed twice in different orientations to check for measurement repeatability.

Both OMA and CMM data were processed using Geomet inspection software. The output data was formatted as two spreadsheets with a part feature on each row and the inspection results arranged by serial number in the columns. This data was processed to remove some unwanted data points and imported into a Microsoft Excel spreadsheet.

### **8.1.2 Phase One Error-Correction Study**

Prior to beginning the error correction study, we addressed machine and probe error to eliminate the introduction of systematic error into the data. The LeBlond lathe was corrected for leadscrew pitch variation and simple backlash because the Fanuc controller is capable of performing these corrections. After implementing the machine and probe error correction, we proceeded to conduct the error-correction study in a manner similar to the benchmark study.

Pre-travel variation, also known as probe lobing, results from non-uniform probing force at different angular orientations of the probe. The variation shows up as an error in the reported probe point. To measure pre-travel variation, a calibration sphere with better than 5 micro-inch sphericity was mounted in the lathe spindle and probed at 5° increments along a longitudinal axis. The resulting set of points was fit with a circle and residual error of the probe points were recorded as pretravel variation. The sphere was measured 5 times, rotated 90° and measured 5 more

times. Geomet was used to compute the center of the measured circle in the X-Z plane. This centering error was then removed from the individual probe points.

Another source of significant systematic error in the benchmark study was measurement error caused by probe-setting error in the X direction. We corrected the probe-setting error using a novel software correction scheme. A calibration sphere was inserted into the lathe spindle and 27 points at 5° increments along a longitudinal axis of the probe were taken without rotating the sphere. Next, Geomet was used to compute the sphere center in the X direction, designated  $X_{0^\circ}$  (see Figure 5.).

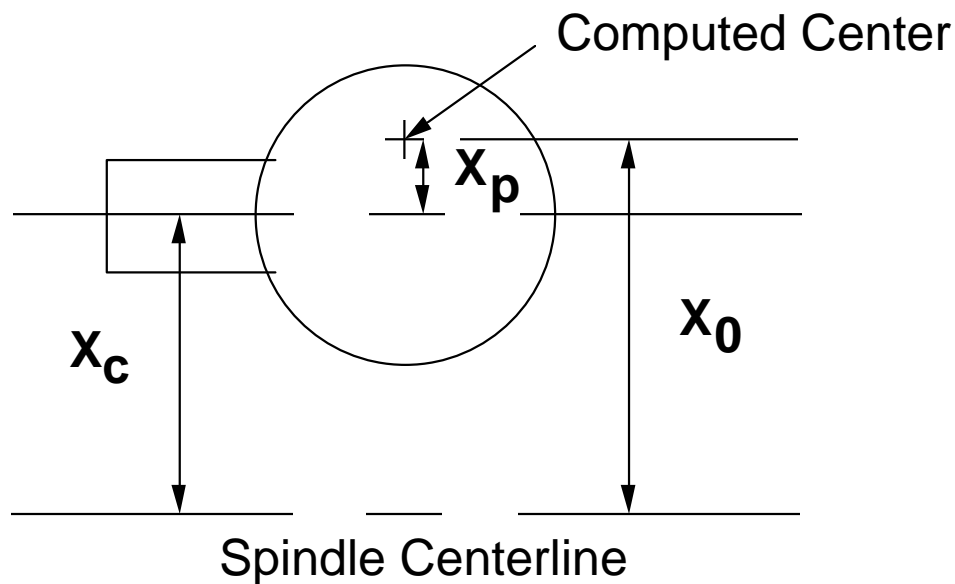


Figure 5. - Probe-Setting in X Direction - Spindle Position = 0°

The spindle was rotated 180° and probed again in the same manner and Geomet was used again to compute the sphere center of the in X, designated  $X_{180^\circ}$  (see Figure 6.). This reversal technique gives the following results:

$$X_{0^\circ} = X_p + X_c \text{ and } X_{180^\circ} = X_p - X_c$$

Where  $X_p$  is the probe offset error and  $X_c$  is the centering error of the sphere in the spindle. These equations in turn give the equation:

$$X_{0^\circ} + X_{180^\circ} = 2X_p$$

The term  $X_p$  can then be subtracted from the probe offset in the X direction to correctly set the probe in the X direction which should, theoretically, give an exact result. In actuality, several iterations of the technique described above may be required to correctly set the probe. Note that due to sphere centering error, the measured locations of the sphere center may still be nonzero in the X direction. After reversal however, the probe-setting error should still be zero.

Modifications to the artifact probing program were made during the error-correction study so that both the probed data point and the standoff point were output to a PC data file. The standoff points were removed using a parsing routine written in C prior to processing the OMI data. Modifying the program allowed compensation for pretravel variation as a function of approach direction. As in the benchmark study, the measurements from both machines were processed using Geomet.

We also reviewed benchmark results with a statistician and reaffirmed that 12 parts would be sufficient to provide a statistically significant sample provided multiple, related features were measured on each artifact. In addition, to test measurement repeatability, artifact serial numbers #SN102, #SN107, and #SN112 were measured three times.

After all the artifacts were machined and inspected on the lathe, they were taken to dimensional inspection. As in the benchmark study, the CMM did not have a rotary table which limited its ability to probe the same points taken on the machine tool.

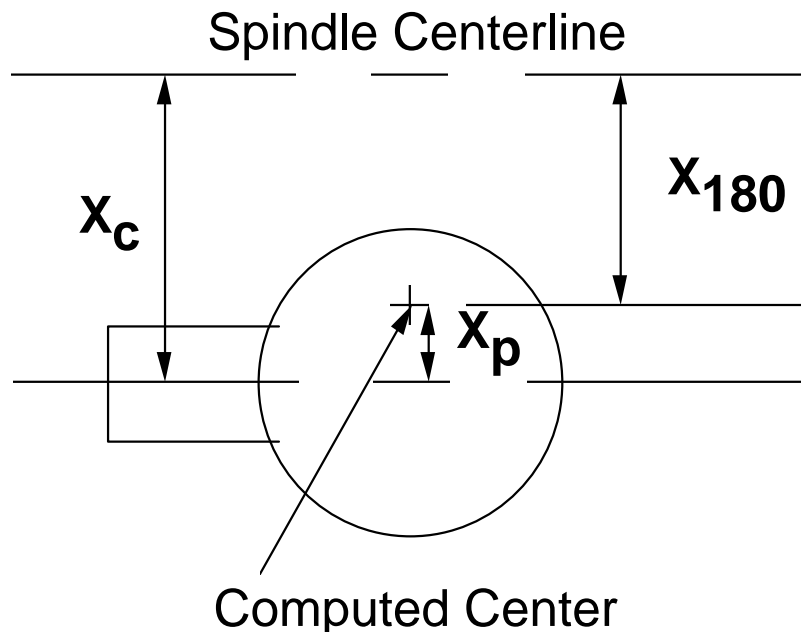


**Figure 6. - Probe-Setting in X Direction - Spindle Position = 180°**

## **8.2 Phase Two Summary**

Phase two of the SNL/CA LDRD included development of an advanced OMA system. An advanced OMA system would need several capabilities including data analysis, interpretation, and visualization to make it useful. <sup>4</sup>

For phase two study, several capabilities were considered necessary when choosing the advanced OMA visualization software. First, the software must be able to render three-dimensional ProEngineer models and overlay an assortment of color-mapped data sets over the model in space. Second, the software must be able to map the sensor data quickly. Third, the software must be able to run on multiple platforms, and fourth, it must have the ability to generate Virtual Reality Modeling Language (VRML) from three-dimensional graphics for the purpose of information exchange between designers and manufacturers. <sup>4</sup>

Phase two of the OMA utilized an assortment of in-process sensors to associate system phenomena with process states. As an example, touch probes are guided along the part surface gathering data to verify part geometry. Real-time data acquisition, rapid data analysis, and visualization of probe data allows the machinist to make the correct decisions about the process while the part is fixtured on the machine tool. The advanced OMA system and three dimensional visualization assists the machinist when making changes to, or interpreting the process status. One method of visualization could be accomplished with color mapping of the three-dimensional sensor data overlaid onto a ProEngineer model of the part. The goal of phase two study was to demonstrate a proof-of-concept for the advanced OMA system. <sup>4</sup>

### **8.2.1 Graphical Visualization of Sensor Data**

Three-dimensional tool force, vibration, acoustic emissions, and torque sensors were mounted to a Haas Mill. Data from these sensors was acquired while the artifact was being machined and the data was transformed and color-mapped onto a ProEngineer part model. Sensor data was then overlaid onto the ProEngineer part. Our goal was an easily read inspection report that a skilled operator could use to make quick accurate decisions about the process while the part is fixtured on the mill. An advanced OMA system with its graphical visualization capability would allow an operator to avoid the pitfalls of interpreting traditional tabled

data reports and two-dimensional graphs. The graphical visualization technique would also give operators a more complete understanding of manufacturing defects that occur during the process. <sup>4</sup>

## 9.0 OMA Time and Cost Analysis

One of the benefits of OMA is the time savings realized from combining the machining and inspection processes. This savings comes from eliminating time spent to normalize the part to 68°F, time in an inspection queue, time spent setting up the part coordinate system, and the time spent actually measuring the part.

An example of the savings that could be realized using the SNL/NM mill stronglink artifact is shown in Table 1. and Figure 7.. Where noted, the times used in the example below are the **actual times required to do machining and inspection** of the mill artifact. The time required to machine and inspect the mill artifact was 76 minutes less than the time required for CMM inspection. Note that the actual OMI took four minutes, but we doubled the inspection time to eight minutes to account for lost spindle time. Suppose the actual mill and CMM time is costed at \$100 per hour and estimated CMM queue and normalize time is costed at \$50 per hour. Then machining and inspection on the mill costs about \$64 per part (38 min./60 min. \* \$100) or \$50 per part (30 min./60 min. \* \$100) if the part is not inspected on the mill. CMM queue and normalize time costs \$75 per part (90 min./60 min. \* \$50). CMM setup and inspection time costs about \$33 per part (20 min./60 min. \* \$100).

Then for a production build of 100 parts, 100% inspected, conventional methods cost about \$15,850  $((\$50 + \$75 + \$33) * 100)$ . The cost to machine and inspect the part on the mill is about \$6350  $(\$64 * 100)$  -- **a savings of \$9500 or 250%**. The reason for this is that about 21% of the part cost can be attributed to inspection in OMA, while about 68% of the part cost can be attributed to inspection using conventional methods.

Note that this comparison does not take into consideration the additional cost of inspection equipment or inspection fixtures, or the maintenance of the equipment and fixtures which also adds to product cost. This example also does not consider the time required for data analysis which should be similar for either machine.

## 10.0 SNL/NM Data Analysis

Data obtained in the OMA study included analysis of thermal data, machine error data, and measurement data. Data obtained from the Zeiss and BostoMatic were evaluated using Microsoft Excel, QUALSTAR, and SAS, a statistical software. Each software provides a different insight about the data and OMA. In addition, we collected metric data on both machines to allow us to carry an additional significant digit in our calculations.

**Table 1. - OMA and Conventional Acceptance Time Requirements**

<b>Time Per Artifact</b>	<b>Zeiss CMM</b>	<b>BostoMatic</b>
Actual Machining Time	---	30 minutes
Estimated Normalize Time	60 minutes	---
Estimated Queue Time	30 minutes	---
Estimated Part Setup	5 minutes	---
Actual Inspection Time	15 minutes	4 minutes
<b>Time Total</b>	<b>110 minutes</b>	<b>34 (38) minutes</b>

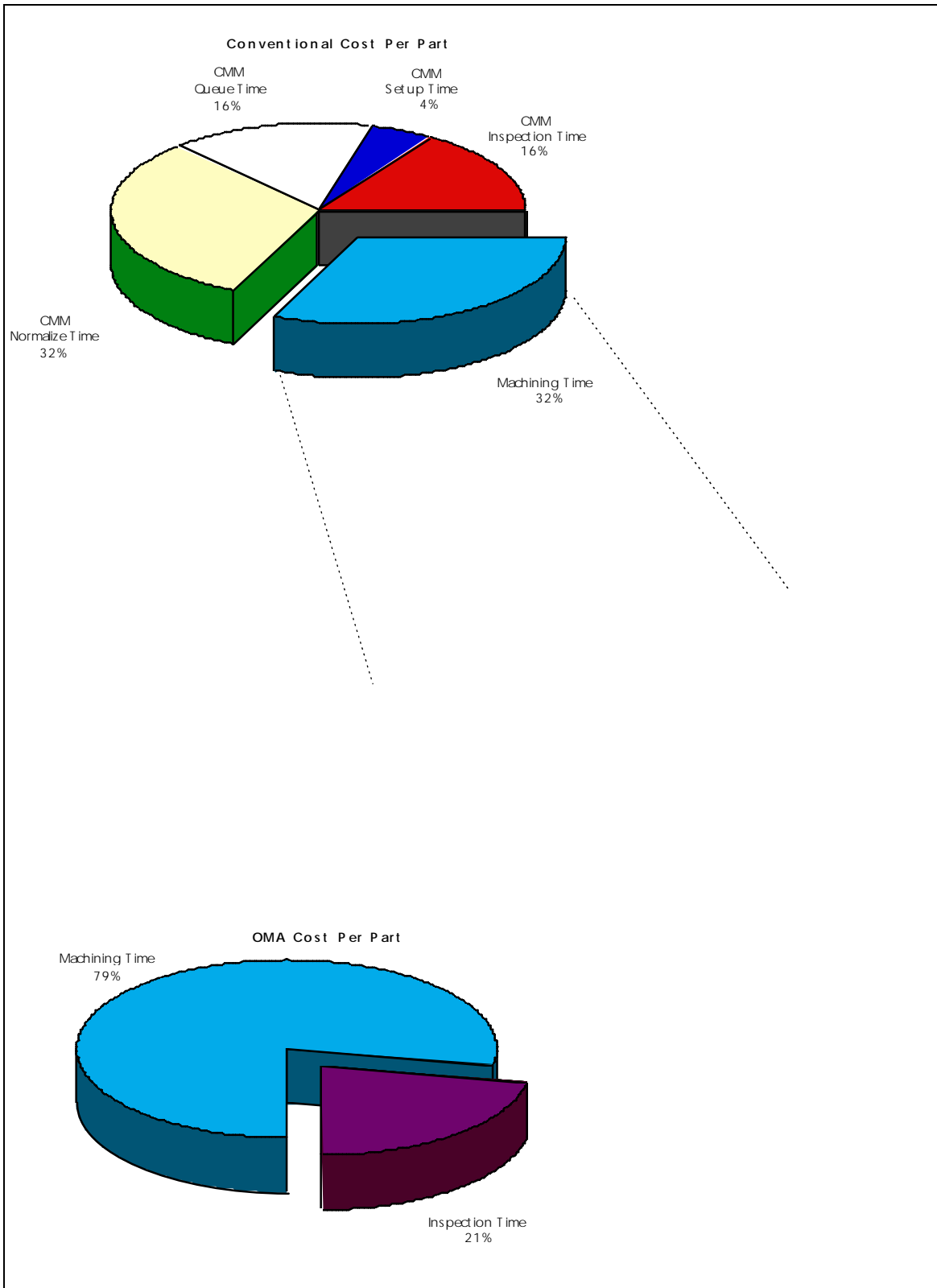


Figure 7. - OMA Cost Savings

## 10.1 Thermal Data Analysis and Summary

Thermal data was collected throughout the machining and inspection process. Six thermocouples were attached to the machine tool at strategic areas on the machine to monitor for thermal impact on the data. Generally, the pattern and thermal responses of the BostoMatic held true for the other days that temperature was monitored. Figure 8. depicts the thermal response of the BostoMatic at the six locations on 3-1-96 that machining and inspection were studied. The location of the six thermocouples were the spindle, servo, Z axis column, table, collet, and coolant tank.

The greatest and most pronounced thermal response occurred in the spindle of the machine which is also the area that could have the greatest impact on machine repeatability. The temperature ranged from approximately 22.5°C to 25.0°C after initial warm-up of the machine. The thermal response in the spindle was consistent and predictable -- usually it rose and fell 2.5°C in 32 - 44 minutes after initial warm-up.

The first of the five measurement runs on the artifact began 6 - 9 minutes after the maximum spindle temperature was attained. All five measurements were completed 8 - 11 minutes after the maximum spindle temperature was attained, but no evidence of greater range in the measurements was obvious.

The servos were the next greatest source of thermal response in the BostoMatic and their temperature ranged from approximately 24.0°C to 26.0°C after initial machine warm-up. The thermal response was less pronounced and less predictable -- the maximum servo temperatures appeared to occur at increasing intervals. In our case, the temperature lag was 75 to 140 minutes, although the temperature ranges remained consistent.

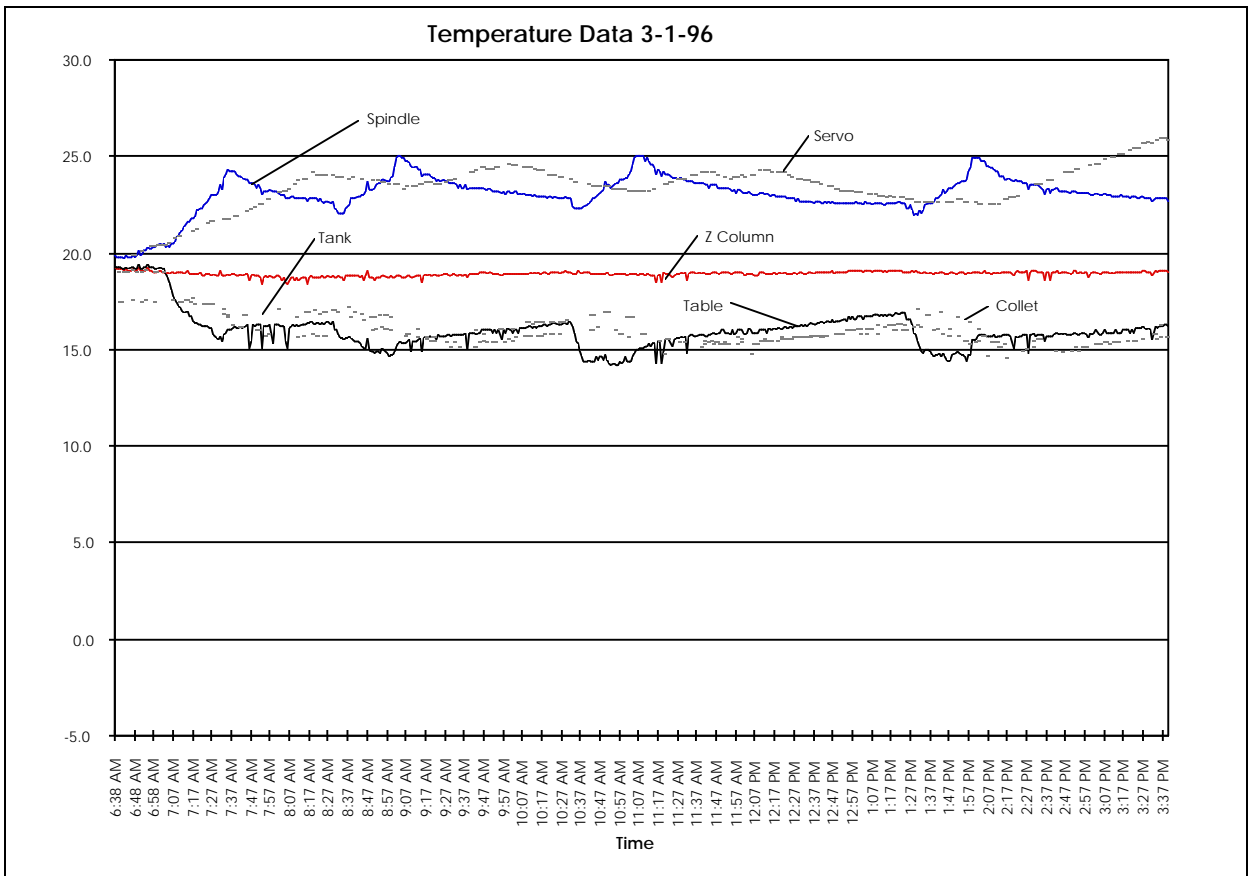


**Figure 8. - BostoMatic Thermal Response - Six Locations**

The Z axis column was the least affected by the machining process with an average temperature range of less than 1°C about 19.0°C after initial machine warm-up. There did not appear to be any correlation between the thermal responses of the spindle and servo and the Z axis column.

The remaining thermocouples were located at the collet holding the artifact, the coolant tank and the table. These temperatures tracked each other very closely ranging between 15.0°C to 17.5°C after initial warm-up of the machine. The maximum difference in these three temperature readings was between the collet and the table. The maximum occurred just after machining and the first measurement of the artifact -- at about 35 minutes. The thermal responses in these three areas of the BostoMatic also appeared to be consistent and predictable. Additionally, there were temperature spikes that appear in the thermal data for the collet and the coolant tank. These spikes were caused by the thermocouples becoming saturated with coolant during machining.

In order to determine how thermal response in the BostoMatic affected our measurement data we evaluated the measurement repeatability in each axis. The thermal expansion for steel is approximately 0.0003 mm per mm per °C (0.0000065" per inch per °F).

The artifact fits into a volume of 41 mm x 41 mm x 6.5 mm (approximately 1.625" x 1.625" x 0.250"). This implies that the maximum that any artifact dimension can increase in any direction due to the 2.5 °C thermal expansion, is 0.0012 mm (less than 0.0005 mm in 41 mm per °C). Both machines have a measurement resolution of only 0.001 mm, so any error introduced into the measurement was lost in the noise of other errors because of the part size. Looking at the range data for the seven artifacts, the range of measurement did not significantly increase with temperature increases, possibly because the size of the part being fabricated and the amount of thermal range seen in the machine. <sup>5</sup>

Our conclusion for this analysis was that our measurement repeatability was not significantly affected by thermal response of the BostoMatic. Some parts of the BostoMatic experienced repeatable and predictable thermal responses for which we believe error correction algorithms can be developed and implemented. Of course, further study is required because thermal response is machine and part dependent, i.e. the size of the part being machined, the time required to machine it, and the size of the machine will drive the amount of error due to thermal response seen in the part measurement.

## 10.2 Machine Error

In order to understand the capabilities of the BostoMatic Milling Machine used in the SNL/NM OMA LDRD effort, we performed an evaluation of the machine tool to the ANSI/ASME B5.54-1992 Standard, "Performance Evaluation of Numerically Controlled Machining Centers".<sup>6</sup> The evaluation of the BostoMatic was used to determine the machine error prior to using the BostoMatic to gather data for three reasons:

- 1.) The information allowed machine-based errors to be isolated from the data collected by the machine so that the true measuring capability of the machine could be evaluated.
- 2.) An error budget for the machine tool could be calculated to allow error correction over the entire working volume of the machine tool as is done in some CMMs.
- 3.) Identifying and quantifying the machine tool errors will allow users to determine the type of the work for which the machine tool is best suited based on its capability.

The data obtained from the ANSI/ASME B5.54 performance evaluation of the BostoMatic was used to perform a machine error analysis. The X axis analysis shown below is also representative of the Y and Z axes. The position errors for all three axes were of the mathematical form:

$$E(\text{position}) = C + P(x) + f(\sin(x), \cos(x)) + R(t)$$

where,

C = a constant error

P(x) = an error approximated by a polynomial

f(sin(x), cos(x)) = a periodic error

R(t) = Random noise

x = the commanded position of the BostoMatic.<sup>7</sup>

During analysis of the data, we observed that the magnitude of averaged error in the X axis were within the manufacturer's published error band for the BostoMatic for approximately 90% of the data. The published error was within a 95% confidence limit for average X values and the predicted next X interval for all data points. Furthermore, the analysis indicated that the average error could be reduced to fall within the published limits if more data were taken on each axis.<sup>7</sup>

### 10.2.1 Machine Error Analysis

Three major machine error types were identified. The first of these was a constant error which could be attributed to initialization or setup errors in the machine zero sensor routine. This constant error was identified in the X axis linear positioning data by comparing the actual and commanded position of the BostoMatic. The constant error was removed from the data to allow polynomial and Fourier modeling of the machine error.

Removing the constant error decreased the magnitude of error in the runs from 0.0009 mm to 0.0006 mm ( $35 \times 10^{-6}$  " to  $24 \times 10^{-6}$  "). The standard deviation was also decreased considerably -- from 0.0008 mm to 0.0002 mm ( $32 \times 10^{-6}$  " to  $9 \times 10^{-6}$  "). Figure 9. illustrates the X axis data prior to removal of the constant error and Figure 10. illustrates the data after removal of constant error. Additionally, the magnitude of the error varied from measurement run to measurement run although the constant error was indeed constant within any particular run. <sup>7</sup>

The second error type was identified in X axis positioning data by investigating second through seventh order polynomials to approximate the error. The second order polynomial was adequate to approximate the linear positioning error (Figure 11.). Removing the polynomial error term decreased the magnitude of positioning errors further from 0.0006 mm to 0.0004 mm ( $24 \times 10^{-6}$  " to  $15 \times 10^{-6}$  "). The coefficients for the 2nd-4th order polynomials are shown in Table 2. for equations of the form,

$$E_j \text{ (estimated)} = \sum_{i=0}^n (C_i * X_j^i)$$

where,

$X_j$  = Commanded linear position at point j

$E_j$  = Positioning error at point j, and

$C_i$  = Calculated polynomial constant. <sup>7</sup>

The polynomial error was suspected to be caused by machine wear - wear in the slides, slide deflection, etc.. This error could be reduced by reconditioning the machine tool, but the machine condition will need to be evaluated periodically to monitor wear, and to update the error model. <sup>7</sup>

The third major source of error was identified via Fourier modeling using a different data set -- the X axis periodic error data set. The change in data sets was necessary because the interval (0.472") in the X axis linear positioning data was too large to determine the true frequency of periodic errors. The X axis period error data had a sampling interval of

0.016" which was better to isolate periodic error using Fourier modeling (Figure 12.). The periodic error was probably caused by backlash, lead screw errors, or drive system errors, but a smaller sampling interval would be more useful in identifying periodic error. The remainder of the error could not be modeled and appears to be random noise. <sup>7</sup>

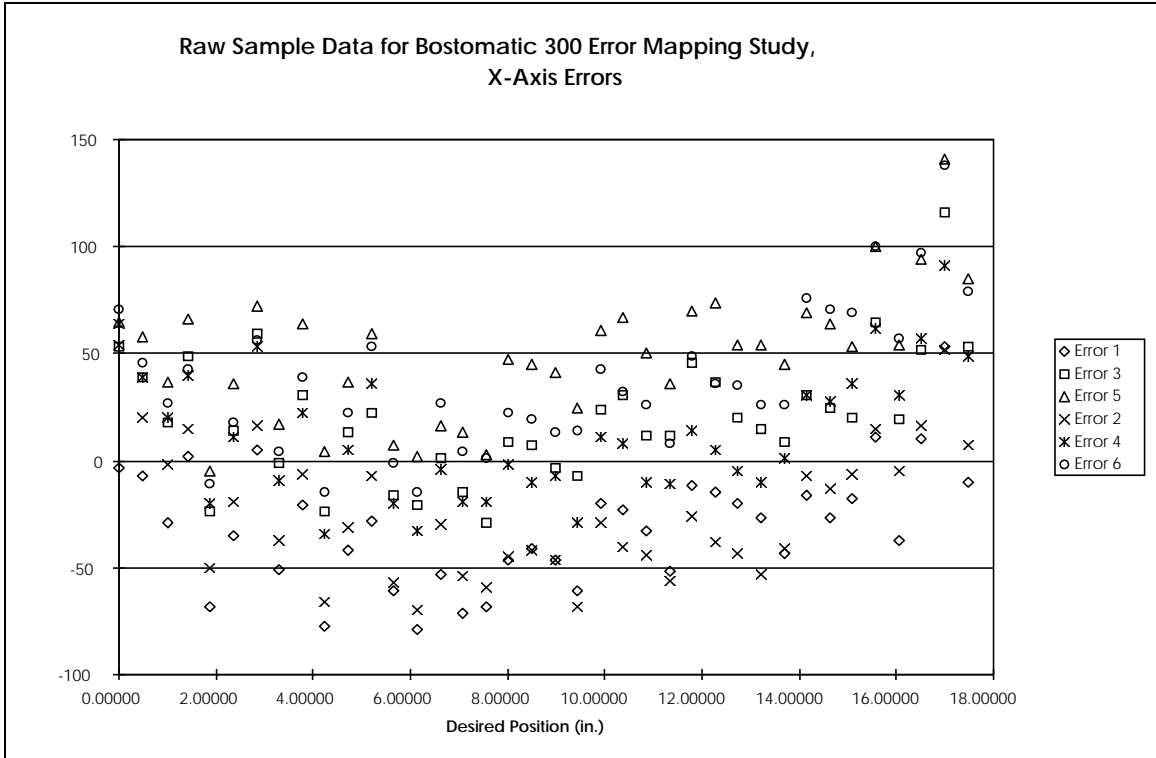
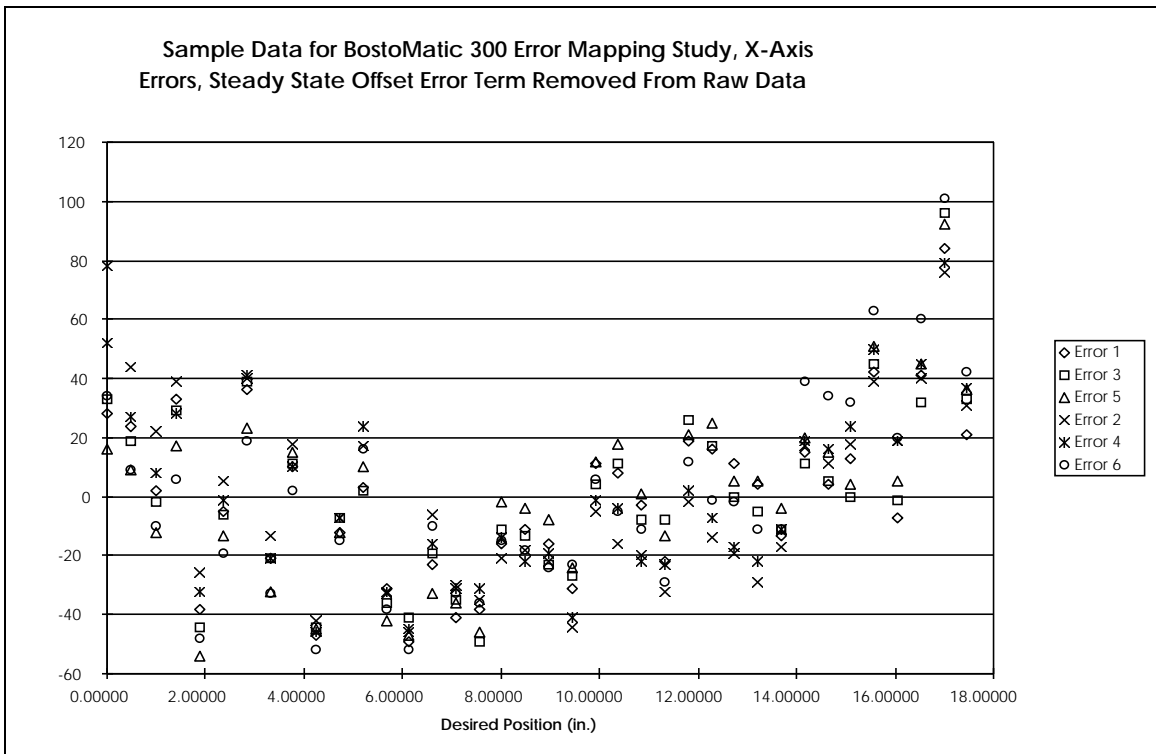


Figure 9. - Raw X Axis Data



**Figure 10. - Steady-State Error Correction of X Axis Data**

### 10.2.2 Machine Error Analysis Summary

For our purposes, we found that the error attributable to the machine error was negligible -- outside the resolution of the BostoMatic, but that approximately 80% of the error could be modeled. Generally, the error analysis indicated that most of the error is repeatable and predictable, given that the time required to identify and model the error is invested. Furthermore, it is possible to model and compensate for this error via error mapping the machine or correction of the data before analysis. Removing sources of repeatable error will enhance measurement accuracy of the machine tool when evaluating the part condition relative to its design requirement.

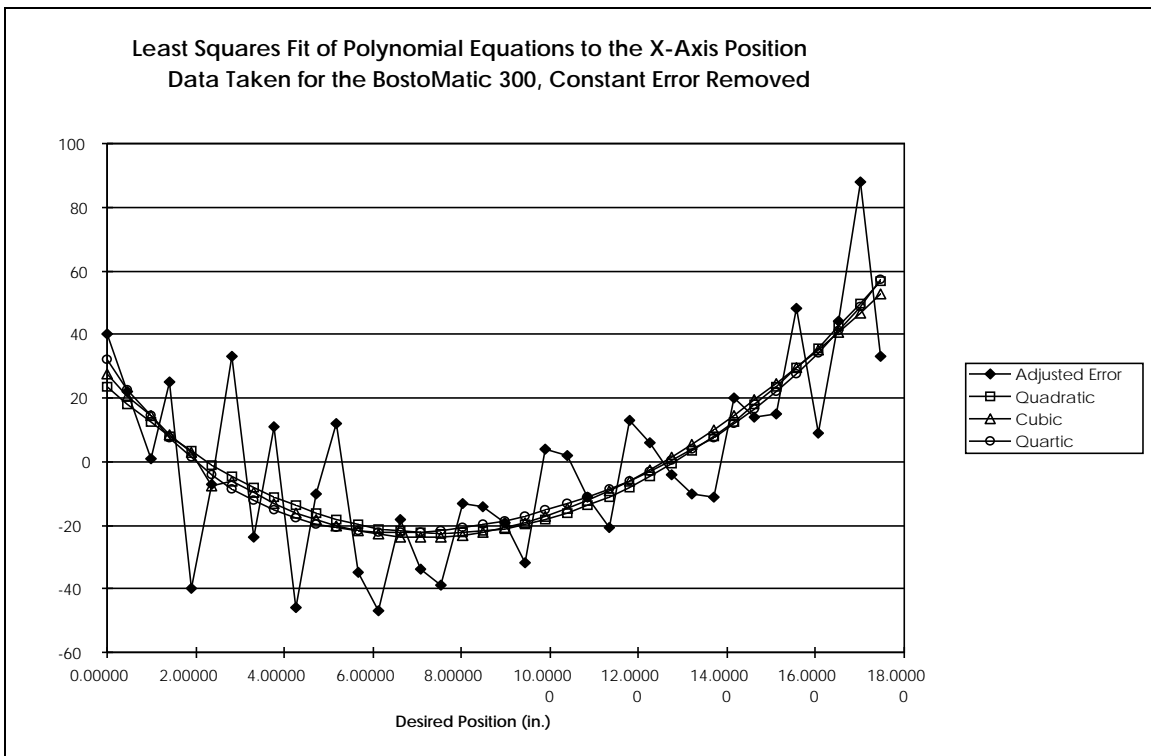


Figure 11. - Steady-State Error Correction and Least Squares Fit Polynomial Equation of X Axis Data

Table 2. - Coefficients for Second Through Fourth Degree Polynomials

n	C	x	X <sup>2</sup>	X <sup>3</sup>	X <sup>4</sup>
2 (Quadratic)	23.42	-12.22	0.809	-	-
3 (Cubic)	27.57	-15.27	1.25	0.0169	-

Intelligent Tools for On-Machine Acceptance of Precision Machined Components

4 (Quartic)	32.13	-21.21	2.83	-0.159	0.00406
----------------	-------	--------	------	--------	---------

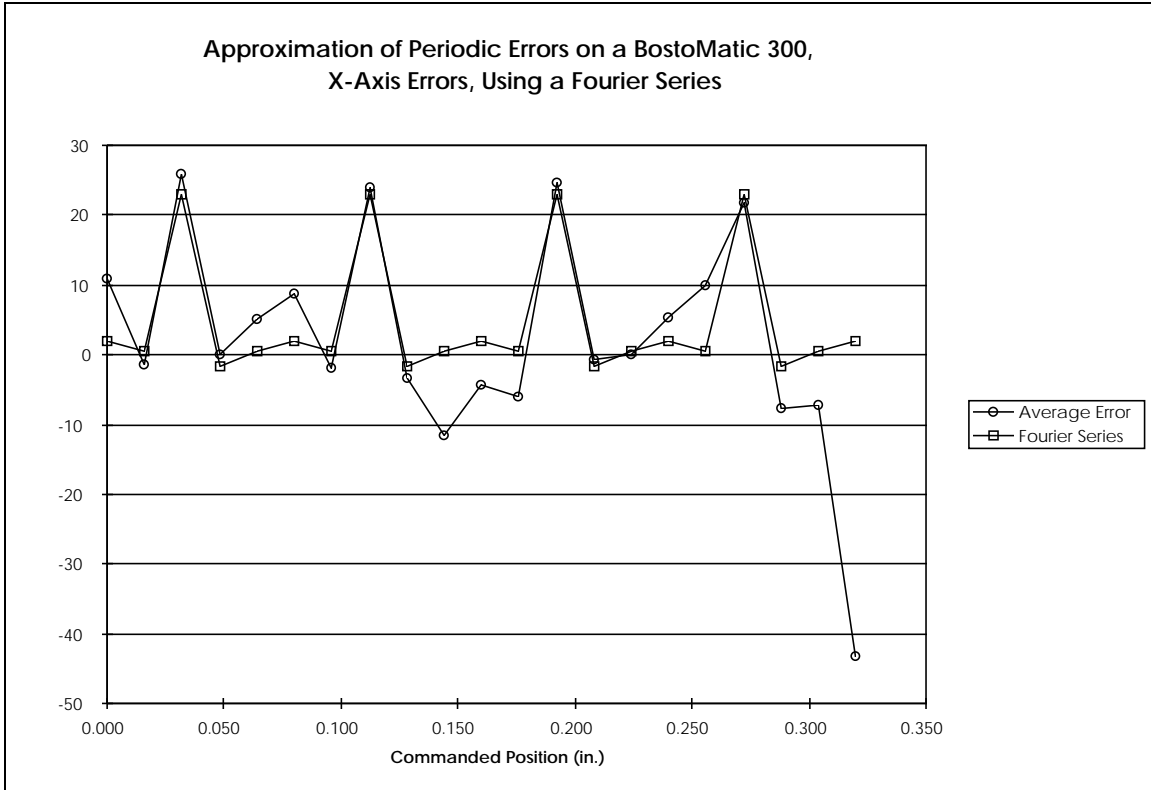


Figure 12. - Fourier Series Periodic Error Modeling of X Axis Periodic Data

### 10.3 Statistical Data Analysis

Two statistical analyses were done to test for significant differences in the mean measurements between the BostoMatic and the Zeiss. First, a three way Analysis of Variance (ANOVA) was performed for each of the X, Y, and Z coordinates. The three factors included in the ANOVA were machine (BostoMatic or Zeiss), points (#1 through #145), and part (artifact #1 through #7). A full model, containing interaction terms was run. <sup>8</sup>

The F-tests for the three-way interaction was highly significant for each of the three dimensions, implying that differences in the means exists for the point by part by machine combinations. Because the F-test is used to test for significantly different means, and it is expected that the different points in the study have different means, these results were not surprising. The test only implies that the comparisons of the means must be done by considering each of the points separately. One method of doing this, while allowing for the fact that the same artifacts were measured on both machines, is to apply a paired comparison t-test. That is, for each point and dimension, the average value over the five runs obtained for artifact #1 on the BostoMatic was compared with the average value for artifact

#1 on the Zeiss. The average value obtained for artifact #2 on the BostoMatic was compared with the average value compared for artifact #2 on the Zeiss, and similar for artifacts #3 through #7. <sup>8</sup>

This type of analysis computes the difference between the BostoMatic and Zeiss average values for artifact #1 through artifact #7 and then uses the resulting seven sample differences to test the hypothesis that the difference is equal to zero. Of course, testing whether the difference in the BostoMatic and Zeiss values was equal to zero is equivalent to testing if the mean values are equal. The p-values resulting from performing these paired t-tests on a point-wise basis for each of the X, Y, and Z coordinates are shown in Table 3.. Blank cells correspond to those points where an axis was set or biased, and thus not really measured. <sup>8</sup>

### 10.3.1 F-Test and Paired t-Test Summary

To summarize the findings, consider first the X-axis. With the exception of points #54, #66, #77, #95, #98, #106, #111, and #119, significant differences at the 0.05 level were found in the mean x-value between the two machines. For the Y-axis, at a .05 level, significant differences were found in the mean values between the BostoMatic and the Zeiss for all points except #54, #66, #77, #95, #111, #119, and #143. On the Z-axis, significant differences were found in the mean values at a .05 level, for all points except #15, #23, #24, #28, and #34. Shaded cells in Table 3. indicate the points that are exceptions to the significant differences. <sup>8</sup>

In summary, it was found that for certain points, there were no significant differences between the mean values obtained on the BostoMatic and those obtained on the Zeiss at a .05 level of significance. For those points where significant differences exists, further research may provide explanations. Techniques such as error mapping and bias correction may be utilized to adjust for the mean differences found at certain points. For example, consider point location #1, where Table 4. provides the average value (taken over the five replications) for the seven parts on both machines taken along the X-axis. <sup>8</sup>

The paired t-test for comparing the mean value between the BostoMatic and the Zeiss is equivalent to using the values in the "difference" column and testing whether the mean difference is equal to zero. From examination of the difference values, was not surprising that the hypothesis test resulted in a p-value less than .0001, implying that the mean difference was not zero and the mean values between the two machines are significantly different. <sup>8</sup>

Note that point 1 is such that the X-axis was biased by the CNC program, and so this significant difference in means appeared to be driven by one of the machines being biased. This was one example where bias

correction techniques could adjust either the BostoMatic or Zeiss values, resulting in no significant differences between means. Applying such correction techniques and investigating points where significant mean differences occur appear to be feasible from this preliminary study. <sup>8</sup>

**Table 3. - P-Values for Points #1 - #145**

Point	p-value X	p-value Y	p-value Z	Point	p-value X	p-value Y	p-value Z
1			0.0001	74			0.0000
2			0.0006	75	0.0000		0.0000
3			0.0016	76	0.0001		
4			0.0144	77	0.1057	0.1509	
5			0.0370	78			0.0000
6			0.0010	79			0.0000
7			0.0054	80	0.0002		
8			0.0002	81			0.0000
9			0.0002	82			0.0000
10			0.0000	83	0.0022		
11			0.0000	84	0.0025		
12			0.0010	85	0.0025		
13			0.0022	86	0.0019		
14			0.0039	87	0.0026		
15			0.7852	88	0.0032		
16			0.0000	89	0.0038		
17			0.0000	90	0.0087		
18			0.0000	91	0.0000	0.0000	
19			0.0009	92			0.0000
20			0.0015	93	0.0000		0.0000
21			0.0001	94	0.0001		
22			0.0000	95	0.0679	0.0789	
23			0.3620	96			0.0000
24			0.9583	97	0.0000		0.0000
25			0.0083	98	0.7987		
26			0.0000	99	0.0000		0.0000
27			0.0002	100			0.0000
28			0.2144	101	0.0000		0.0000
29			0.0000	102	0.0000		
30			0.0246	103	0.0375	0.0491	
31			0.0001	104			0.0000
32			0.0344	105	0.0000		0.0000
33			0.0086	106	0.1115		
34			0.3999	107	0.0000		0.0000
35			0.0000	108			0.0000
36			0.0000	109	0.0000		0.0000
37			0.0010	110	0.0000		
38	0.0001			111	0.1494	0.1494	
39	0.0279	0.0279		112			0.0000
40		0.0000		113	0.0011		0.0013
41	0.0000	0.0000		114	0.0089		
42	0.0039			115	0.0000		0.0000
43	0.0002	0.0002		116			0.0000
44		0.0000		117	0.0000		0.0000
45	0.0000	0.0000		118	0.0000		
46	0.0037			119	0.4091	0.4091	
47	0.0002	0.0002		120			0.0382
48		0.0000		121	0.0000		0.0000
49	0.0000	0.0000		122	0.0483		
50	0.0001			123	0.0000		0.0000
51	0.0096	0.0096		124			0.0000
52		0.0000		125	0.0000		0.0000
53	0.0000	0.0000		126	0.0001		
54	0.1392	0.2099		127	0.0371	0.0416	
55	0.0001			128			0.0000
56	0.0000	0.0000		129	0.0000		0.0000
57		0.0000		130	0.0021		
58	0.0002	0.0002		131	0.0001		
59	0.0037			132	0.0000		0.0000
60	0.0000	0.0000		133	0.0000		0.0000
61	0.0000	0.0000		134			0.0000
62	0.0037	0.0239		135			0.0467
63	0.0021			136	0.0000		0.0000
64	0.0000	0.0000		137	0.0000		0.0000
65		0.0000		138	0.0016		
66	0.0549	0.0668		139	0.0002		
67	0.0002			140	0.0000		0.0000
68	0.0000	0.0000		141	0.0000		0.0000
69	0.0000	0.0000		142			0.0000
70	0.0000	0.0000		143			0.1815
71	0.0000	0.0000		144	0.0000		0.0000
72	0.0017			145	0.0000		0.0000
73	0.0001	0.0001					

**Table 4. - Average Values and Differences - BostoMatic vs. Zeiss in Point #1 (mm)**

Part	BostoMatic	Zeiss	Difference
Part #1	19.7480	19.7485	-0.0005
Part #2	19.7480	19.7485	-0.0005
Part #3	19.7480	19.7485	-0.0005
Part #4	19.7480	19.7485	-0.0005
Part #5	19.7480	19.7485	-0.0005
Part #6	19.7480	19.7485	-0.0005
Part #7	19.7480	19.7485	-0.0005

The other important consideration was determining what constituted a “practical” difference in mean values between the two machines. If the replication error is quite small for each machine in contrast to the error between machines, then hypothesis testing may result in the conclusion that significant mean differences exist. However, it may be questionable, for actual applications whether the error between machines is of practical significance. <sup>8</sup>

#### 10.4 Uncorrected and Corrected Data Analysis

Three types of analysis were done on the artifact and calibration sphere data using MicroSoft Excel. The three analyses were:

- 1.) Verification of measurement accuracy on the uncorrected artifact data,
- 2.) Verification of measurement accuracy on the corrected calibration sphere and artifact data, and
- 3.) Verification of measurement repeatability on the uncorrected calibration sphere and artifact data.

Data from artifact #1 and the sphere probed immediately before artifact #1 was probed was used in Figures 13. through 23. and Tables 5. and 6.. Artifact #1 illustrated general observations and trends seen the data from the other six artifacts that were machined, except where noted. None of these data are error-corrected for approach or retract vector differences, thermal effects, probe error, or machine error. Figures 13. through 23. and Tables 5. and 6., illustrate raw data only and error correction will certainly improve the results. Detailed data and graphics for the other artifacts are documented in SAND96-2631, “Laboratory Directed Research and Development - Intelligent Tools for On-Machine Acceptance of Precision

Intelligent Tools for On-Machine Acceptance of Precision Machined Components

Machined Components - Data Sets", N. G. Christensen, L. D. Harwell, A. Hazelton. <sup>5</sup>

It is important to note for data analysis purposes that the significant digits captured in the metric data were different for the Zeiss and the BostoMatic. The BostoMatic only measured to three significant metric digits while the Zeiss measured to four significant digits. Five significant digits were carried forward in all calculations although only four of these are significant.

#### 10.4.1 Accuracy Analysis

The accuracy of the uncorrected BostoMatic data was analyzed by comparing it to the Zeiss CMM measurements. **This analysis assumed that the Zeiss was a master measurement system that produced accurate data.** Figure 13. illustrates the degree of measurement difference in each of the three axes. The average X, Y, and Z values were obtained from the five separate measurement runs for both Zeiss and BostoMatic. The accuracy of the BostoMatic was obtained by taking the absolute value of the average differences in X, Y, and Z data values at each of the 145 artifact points.

There are several items of interest in this graphic. Note that the worst case differences in the measurements are approximately 0.1 mm (0.004") and occur in the Y axis. The X axis shows the next greatest difference, while the Z axis shows the least difference. Another observation is that the differences in the X and Y measurements exhibit cyclic patterns. The peaks and valleys occur while probing circles. Points where the difference is equal to zero are points where the X, Y, or Z axes were "set" or biased by control of the CNC program. Probing occurs in one axis or direction only and the other axis is held steady by the CNC program. For example, while probing at 0° on a circle, the X axis is driving towards the part in the +X direction and the Y axis is controlled (set) by the probing program to some nominal value. The set Y value varies very little (resulting in a difference of zero) as shown in Figure 13. while the probed X direction shows variation about the nominal value. Set (zero) values for the X and Y axes are 90° out of phase.

The difference in the X and Y measurements peaks when either machine is probing at 45° from the X or Y axis, at 45°, 135°, 225°, and 315° on circles, for example. Increased differences occur because at these locations, both the Zeiss and BostoMatic drive in two directions simultaneously trying to maintain the nominal probe location as directed by the CNC probing program. At these locations, both X and Y axes are taking valid data that is not biased to zero values. The greater differences at 45° intervals illustrate the inability of the machine to probe in the exact the location

specified by the CNC program. Peak values for the X and Y axes are also 90° out of phase.

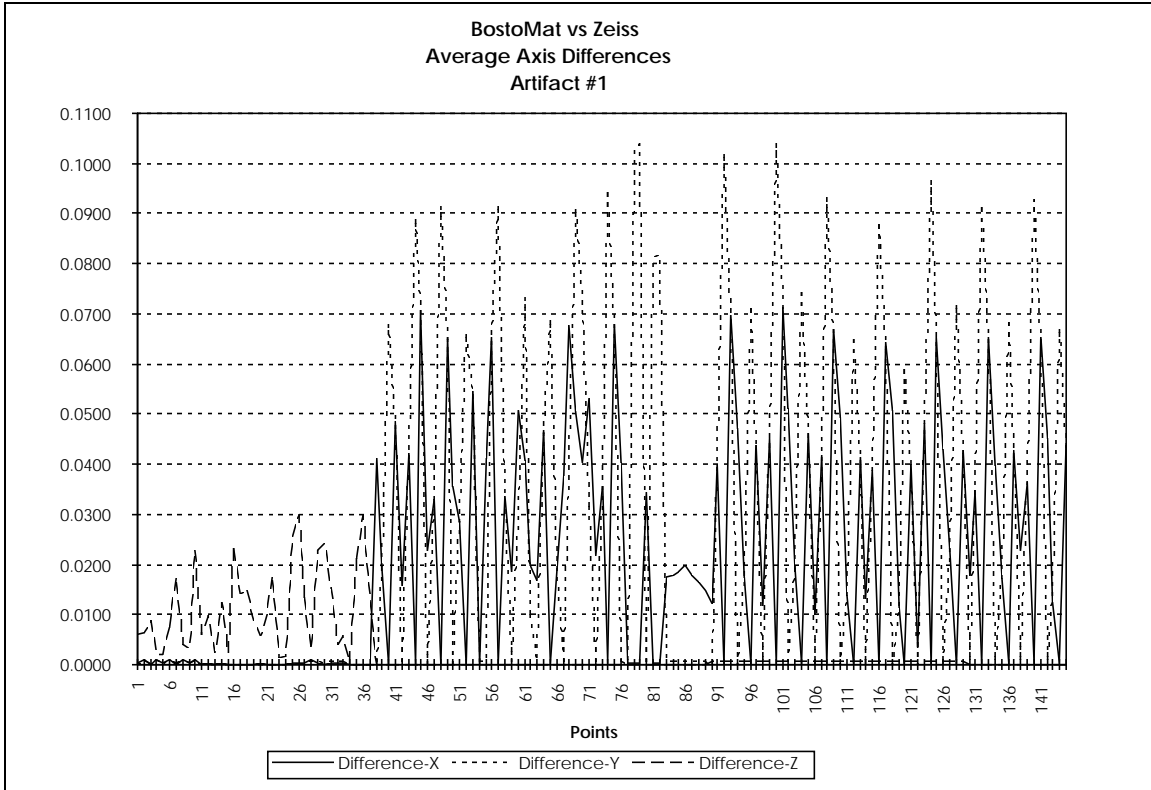


**Figure 13. - BostoMatic Accuracy - Comparison of Average Uncorrected Artifact Values**

Data for the standard sphere was not run through a similar analysis because the sphere locations (centers) on the BostoMatic and Zeiss were not established as they were for the artifact. Because the sphere centers were not established and were not identical, the X, Y, and Z axis values were different and could not be subtracted to obtain valid accuracy data. This analysis could be done by running the data through a transform matrix or a CMM measurement package.

The second analysis was to determine whether the measurement accuracy could be improved by correcting the data for displacement error. QUALSTAR “best fits” data to a nominal part model and creates a normal vector from the nominal artifact model surface to the actual data point or actual part surface. This normal vector may be positive or negative depending on the condition of the artifact -- a negative vector indicates an absence of material while a positive vector indicates a surplus of material. QUALSTAR then displays the normal vector as a “whisker” on the part whose length varies according to the positive or negative deviation from nominal. After running the average artifact data

from both machines through QUALSTAR, the agreement between the two measurements improved considerably (Figure 14.).

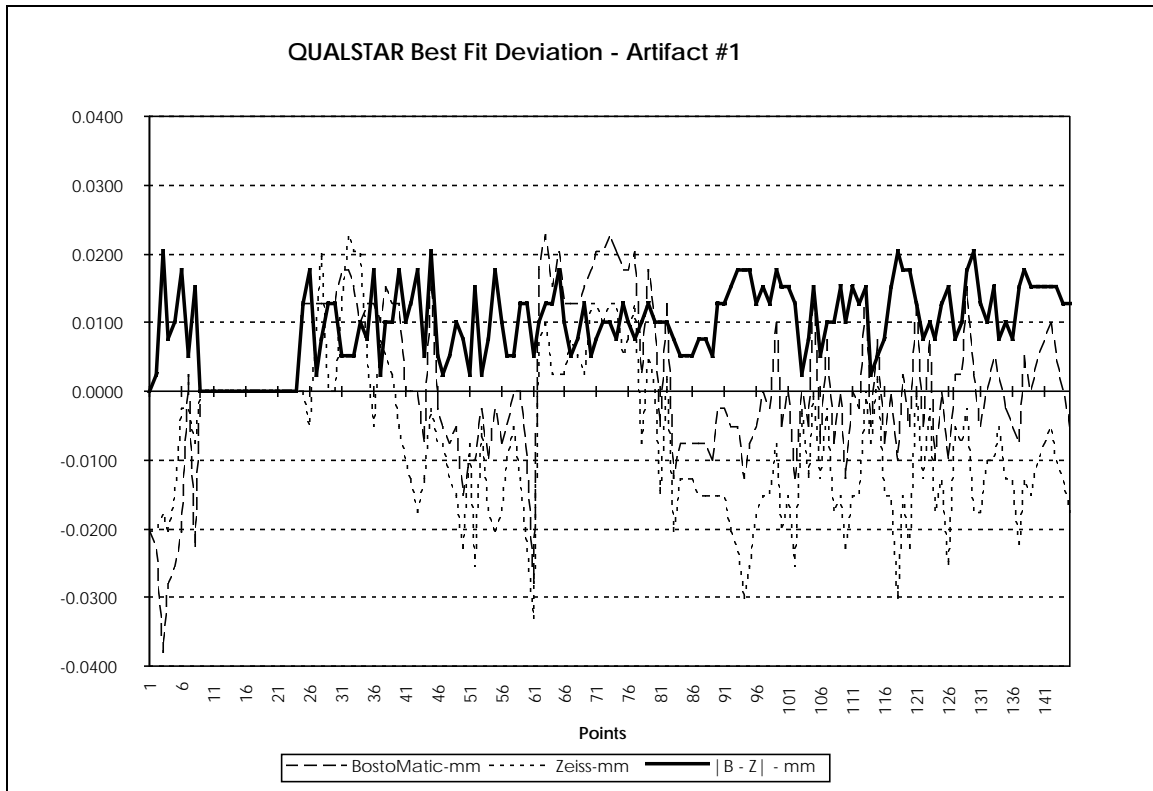


**Figure 14. - BostoMatic Accuracy - Comparison of Average Corrected Artifact Values**

There are also several items of interest in this corrected data. First, the vectors associated with each machine "track" each other well, i.e. both machines detect an absence or surplus of material in the same locations. Generally, the BostoMatic measured the artifact larger than the Zeiss did, possibly because of the probing direction or overtravel. Figure 14. illustrates the length of the normal vector for both the Zeiss and BostoMatic measurements (dashed lines). Also shown (bold line) is the absolute value of the difference between the Zeiss and BostoMatic vectors.

**Note that the worst case differences in the measurements have decreased by an order of magnitude to approximately 0.02 mm (0.0008").** We believe that the improvement in accuracy shown in Figure 14. is due to the fact QUALSTAR "best fits" data to the nominal part model coordinate system. The ability of the Zeiss to establish a valid coordinate system for the artifact is probably responsible for the 0.1 mm difference in part measurement in the first analysis. Once the data was attached to the artifact model coordinate system, and was no longer dependent on the coordinate systems created by the BostoMatic or established by the Zeiss, the differences between the two "best fits" of the data decreased.

The 0.02 mm difference obtained by using QUALSTAR should be improved further if error correction for temperature, machine error, and probe error are implemented. We also assumed that the measurement differences of the corrected X, Y, and Z deviations comprising the QUALSTAR normal vector must be smaller than the X, Y, and Z deviations for the uncorrected measurements, but the separate axes were not studied in this analysis.

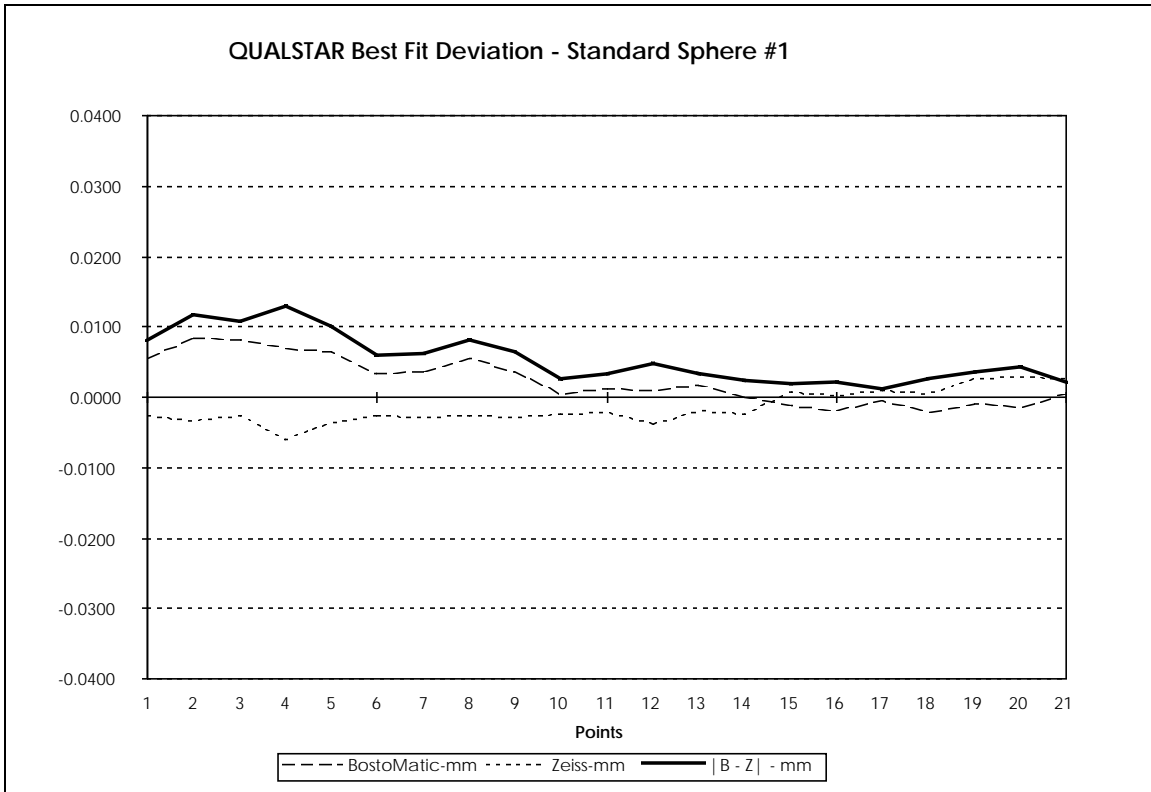


**Figure 15. - BostoMatic Accuracy - Comparison of Average Corrected Standard Sphere Values**

The next analysis was to study the differences between the two machines in measurement of the standard 22.225 mm (0.875") sphere after the data was processed using QUALSTAR. For comparison, Figure 15. shows the amount of deviation at the same scale on the standard sphere for the 21 points probed. The length of the normal vector for the Zeiss and BostoMatic measurements are shown as dashed lines and the absolute value of the difference between the vectors is shown as a bold line. The worst case differences in the measurements have decreased to approximately 0.013 mm (0.0005"), i.e., the ability of the machines to measure the part and give the same result has been improved on the standard.

Besides the improvement in accuracy, we also observed a tendency for the Zeiss to measure the sphere smaller at its "equator" than BostoMatic did for all but one data set. At about 45° from the "equator", the differences were about 0.001 mm (0.00004"). As the probed points approached the "pole" of the sphere, the BostoMatic began to measure the sphere smaller than the Zeiss did although difference was less than 0.005 mm (0.0002"). We have not determined the cause of this observed tendency, but it could be due to the difference in how the data is acquired, i.e., the differences in probing direction.

#### 10.4.2 Repeatability Analysis

The method used to determine the repeatability of the BostoMatic was not dependent on the use of the Zeiss as a measurement standard. The repeatability data was obtained by determining the range of five measurement runs for each of the 145 points. The results of the repeatability analysis for the seven artifacts could not be generalized to the same degree as the accuracy analysis results, but detailed information can be found in SAND96-2631. <sup>5</sup>

Table 5. illustrates the worst case range and sigma in the X, Y, and Z axes for each of the 145 points probed on the artifact. The artifact listed as #7A is the same artifact as #7 except that the probe was removed from the spindle of the BostoMatic and reinserted prior to each measurement run. This removal was done to study the ability to repeat location of the probe into the machine tool.

A problem occurred on point #113, artifact #2 while probing a circle which increased the X and Y axes worst case range to 0.114 mm, but no cause for the problem could be identified. A problem also occurred on point #30, artifact #4 while probing a plane in the Z axis. This problem could be attributed to a burr on the artifact that was large enough to prevent the BostoMatic probing program from running properly. The other four artifacts showed ranges comparable to artifact #1. Also note that removing and replacing the probe in the machine spindle had the effect of increasing the worst case error range on artifact #7.

Table 6. illustrates the worst case range and sigma in the X, Y, and Z axes for each of the 21 points probed on the standard sphere. The fewer number of points and the use of a standard decreased the worst case range to 0.007 mm (0.00027") for all axes. As with the artifact, removing and replacing the probe in the machine spindle had the effect of increasing the worst case error range on the standard sphere prior to probing artifact #7. Generally, for all artifacts, the measurement range of

the Zeiss was less than the BostoMatic for both the artifact and standard sphere.

**Table 5. - Worst Case BostoMatic Artifact Range and Sigma (mm)**

<u>Part #</u>	<u>Max X Range</u>	<u>Max Y Range</u>	<u>Max Z Range</u>	<u>Max X Sigma</u>	<u>Max Y Sigma</u>	<u>Max Z Sigma</u>
1	0.00800	0.00800	0.00300	0.00363	0.00342	0.00141
2	0.11400	0.11400	0.00300	0.05704	0.05691	0.00110
3	0.00500	0.00600	0.00500	0.00230	0.00239	0.00217
4	0.04800	0.06200	0.21000	0.02115	0.02762	0.10817
5	0.00700	0.00500	0.00500	0.00261	0.00182	0.00207
6	0.00600	0.00500	0.00300	0.00259	0.00217	0.00130
7	0.00200	0.00600	0.00200	0.00100	0.00251	0.00110
7A	0.01200	0.01400	0.00200	0.00526	0.00631	0.00100

**Table 6. - Worst Case BostoMatic Standard Sphere Range and Sigma (mm)**

<u>Part #</u>	<u>Max X Range</u>	<u>Max Y Range</u>	<u>Max Z Range</u>	<u>Max X Sigma</u>	<u>Max Y Sigma</u>	<u>Max Z Sigma</u>
1	0.00700	0.00700	0.00400	0.00297	0.00311	0.00164
2	0.00700	0.00400	0.00300	0.00259	0.00164	0.00152
3	0.00400	0.00400	0.00400	0.00179	0.00148	0.00167
4	0.00200	0.00300	0.00300	0.00084	0.00110	0.00122
5	0.00600	0.00400	0.00400	0.00249	0.00167	0.00164
6	0.00700	0.00500	0.00300	0.00270	0.00207	0.00130
7	0.00400	0.00300	0.00300	0.00167	0.00114	0.00152
7A	0.01200	0.00900	0.00800	0.00607	0.00467	0.00374

Figures 16. and 17. illustrate the degree of repeatability of the two machines in the X axis on both the artifact and the standard sphere. Figures 18. and 19. and Figures 20. and 21. illustrate the degree of repeatability of the two machines in the Y and Z axes on both artifact and sphere, respectively. Generally, the BostoMatic and the Zeiss ranges were of the same order of magnitude with the BostoMatic having slightly greater ranges for the five measurement runs.

There are several items of interest to observe in these graphs. First, for all three axes, the worst case repeatability of the BostoMatic while measuring artifact #1 was 0.008 mm (0.00032") or less while the Zeiss worst case was 0.005 mm (0.00020") or less. The worst case repeatability of the BostoMatic while measuring the standard sphere was 0.007 mm (0.00028") or less while the Zeiss worst case was 0.002 mm (0.00008") or less. The Z axis

showed the best repeatability, and the X and Y axes showed about the same degree of range variability.

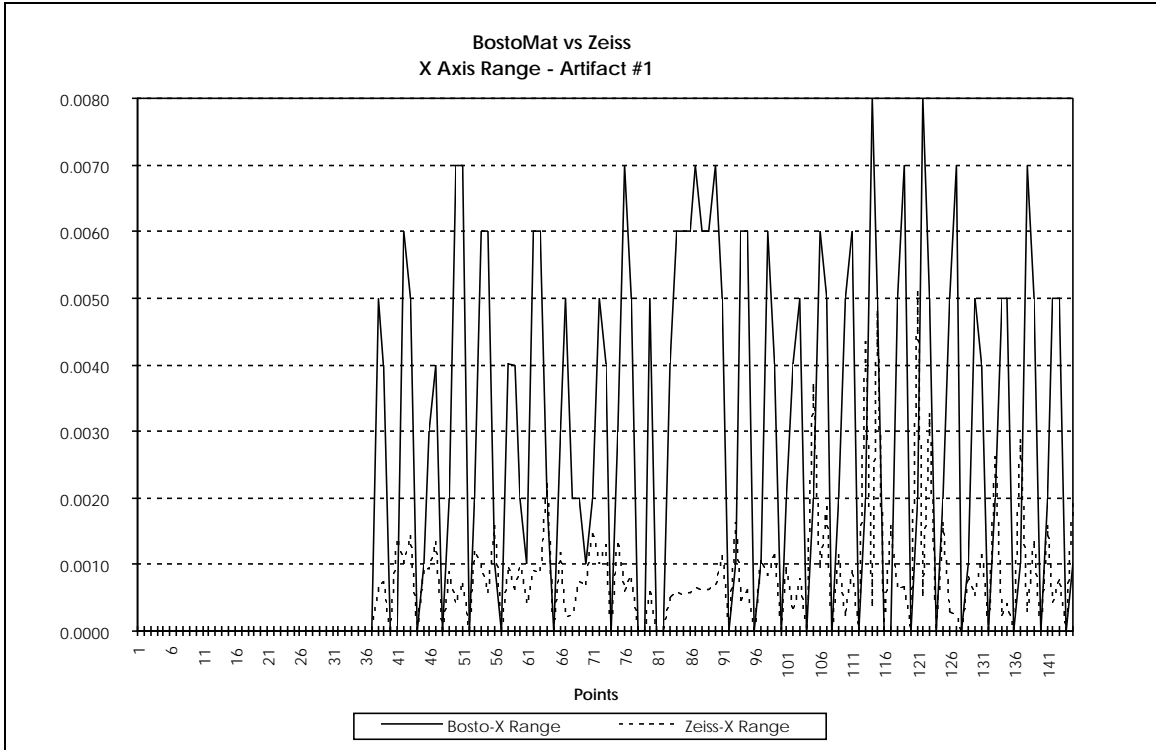
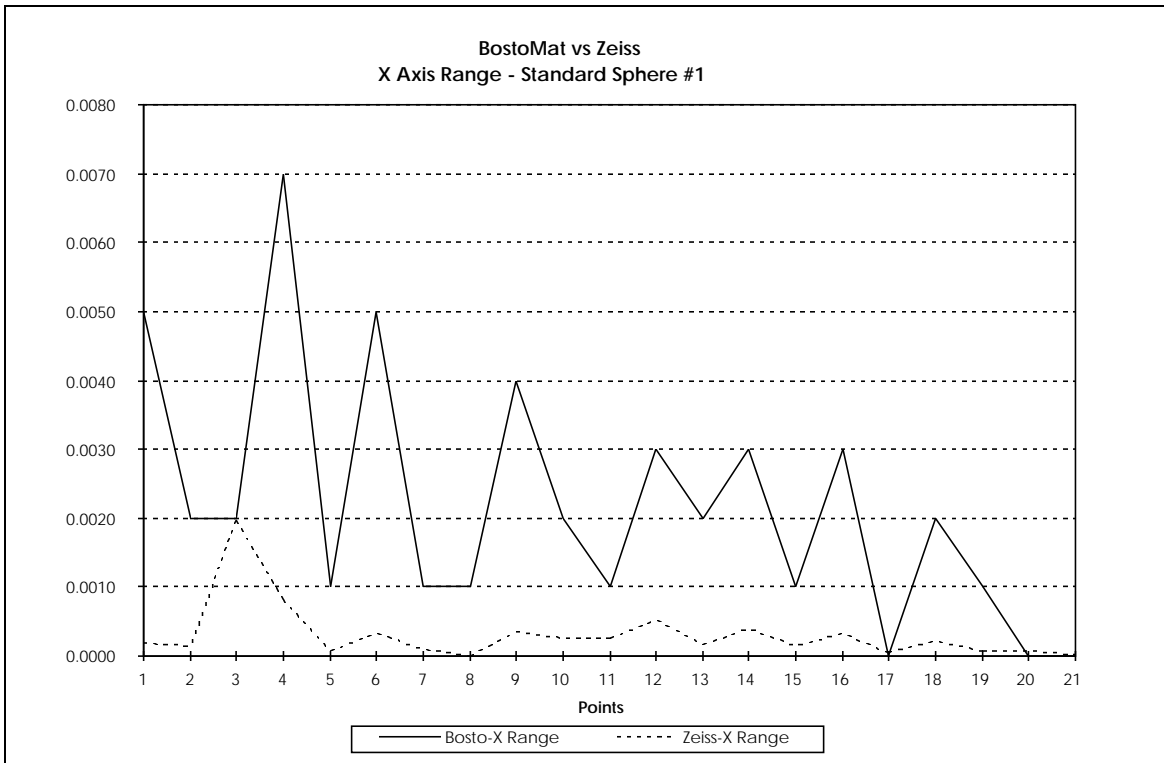


Figure 16. - BostoMatic vs. Zeiss - X Axis Range on Artifact



**Figure 17. - BostoMatic vs. Zeiss - X Axis Range on Standard Sphere**

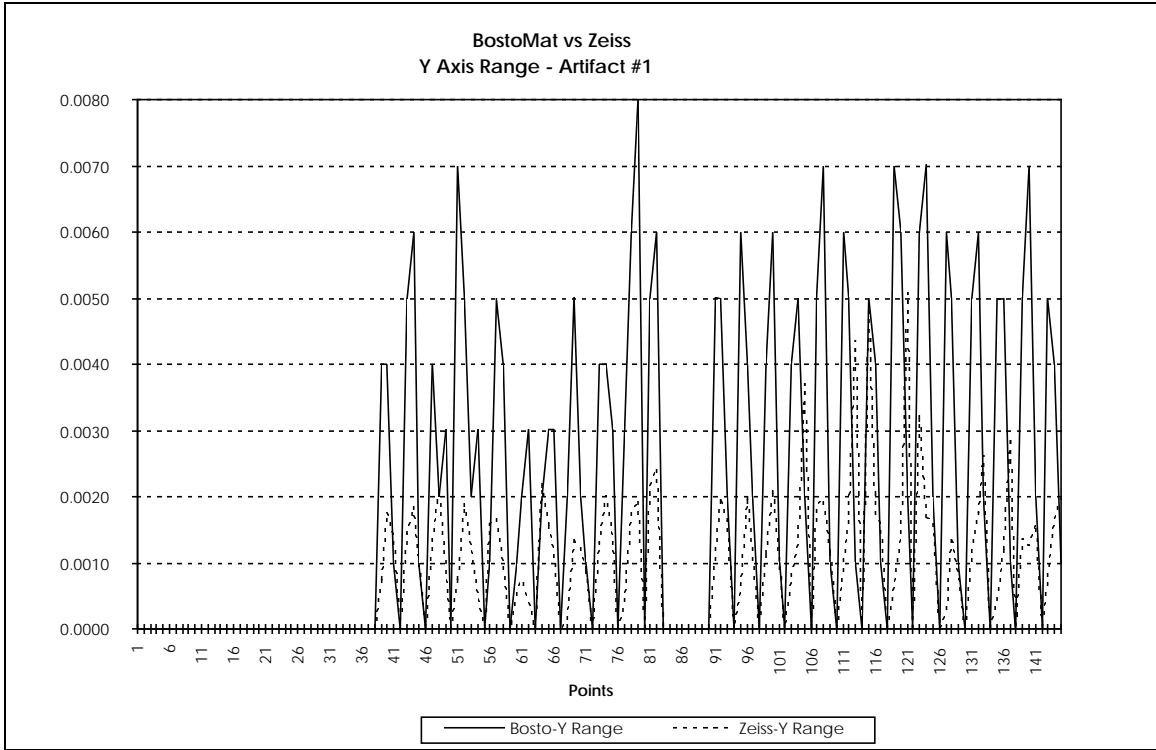
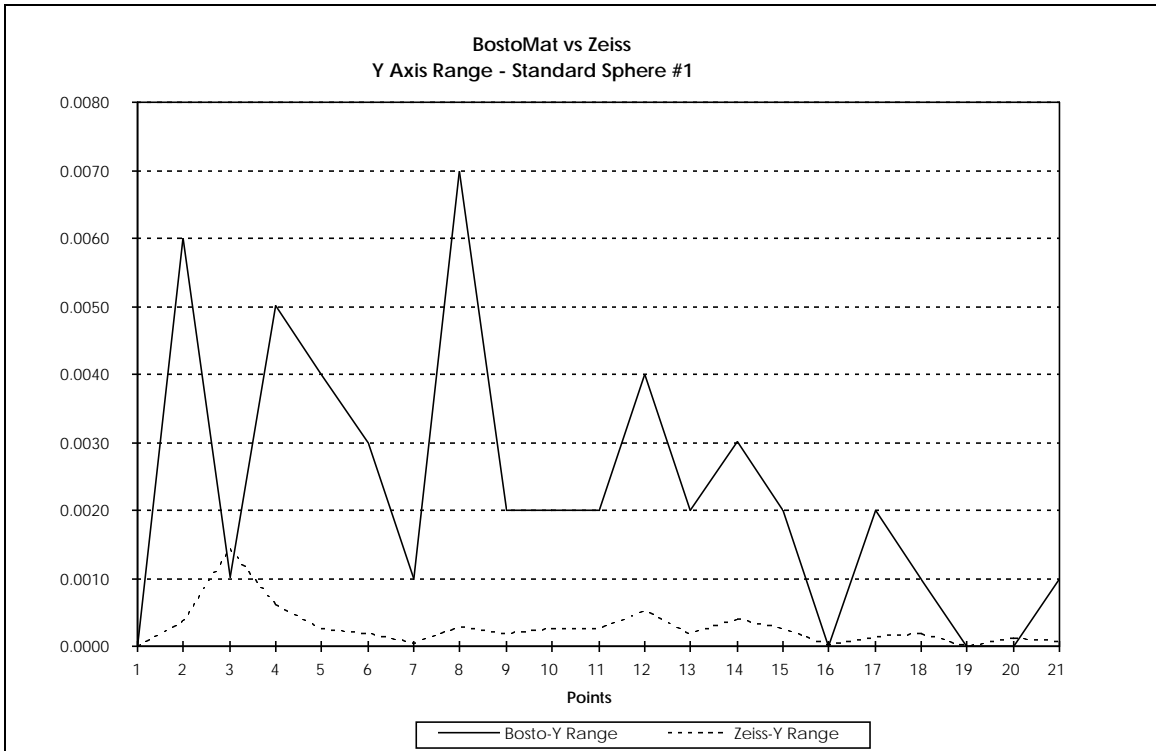


Figure 18. - BostoMatic vs. Zeiss - Y Axis Range on Artifact



**Figure 19. - BostoMatic vs. Zeiss - Y Axis Range on Standard Sphere**

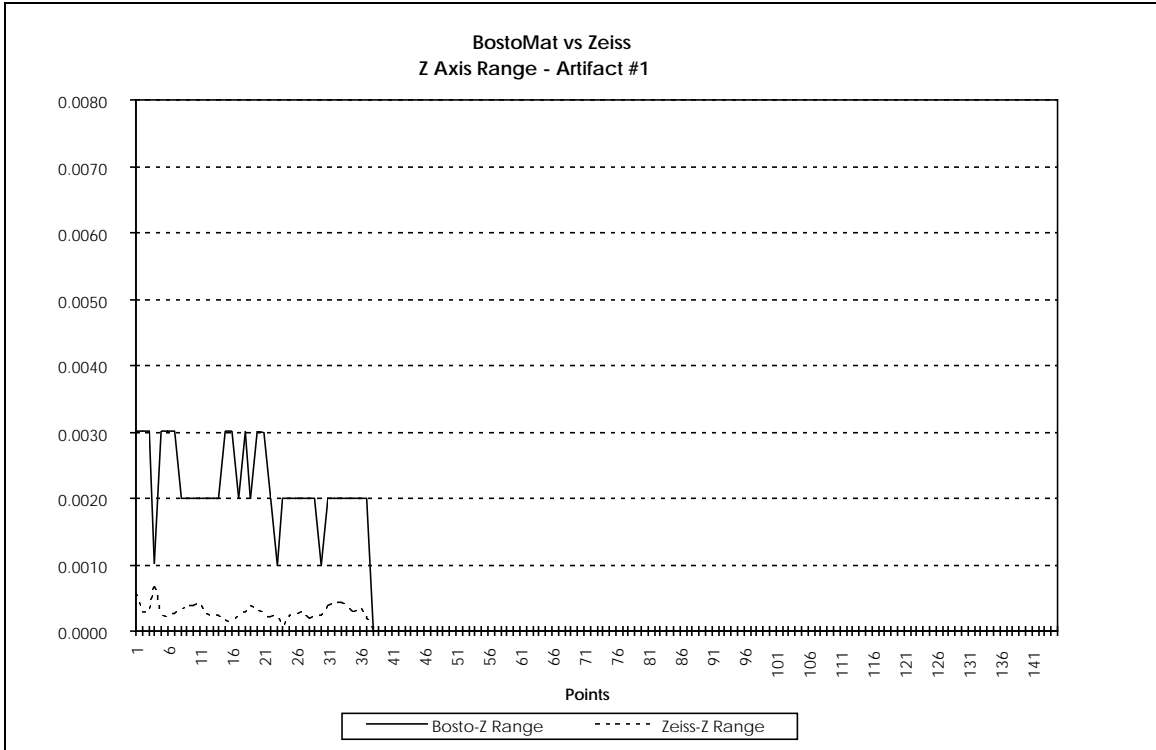
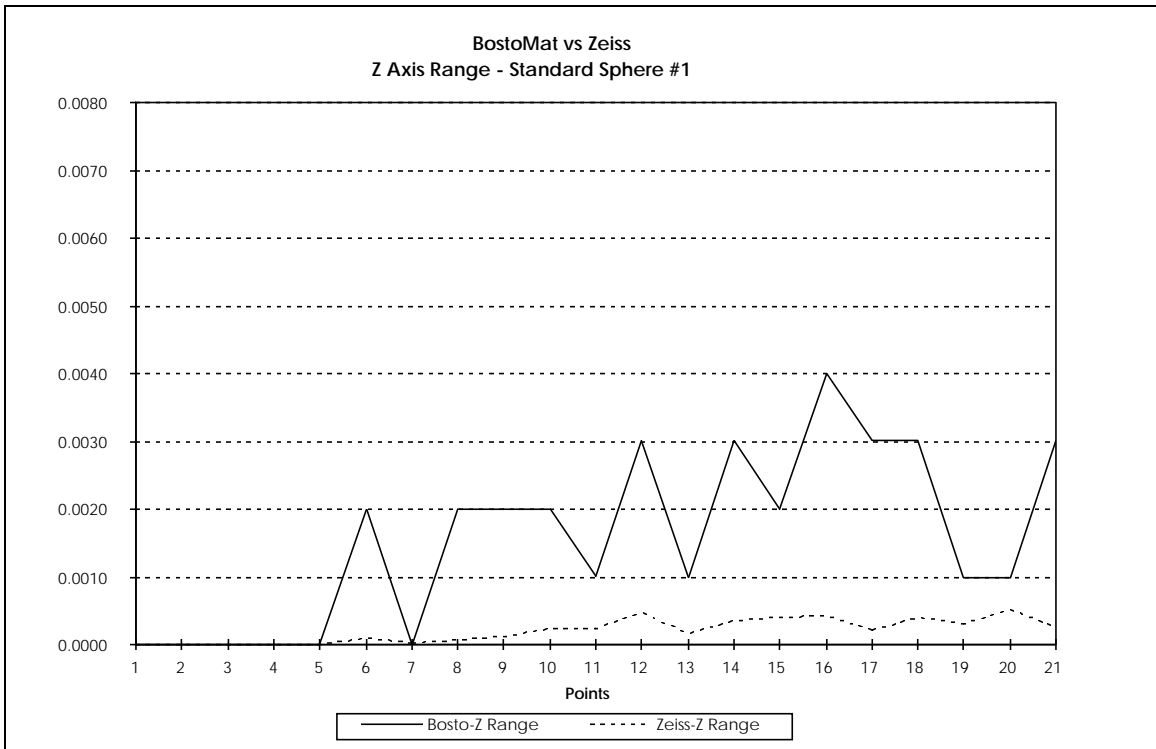


Figure 20. - BostoMatic vs. Zeiss - Z Axis Range on Artifact



**Figure 21. - BostoMatic vs. Zeiss - Z Axis Range on Standard Sphere**

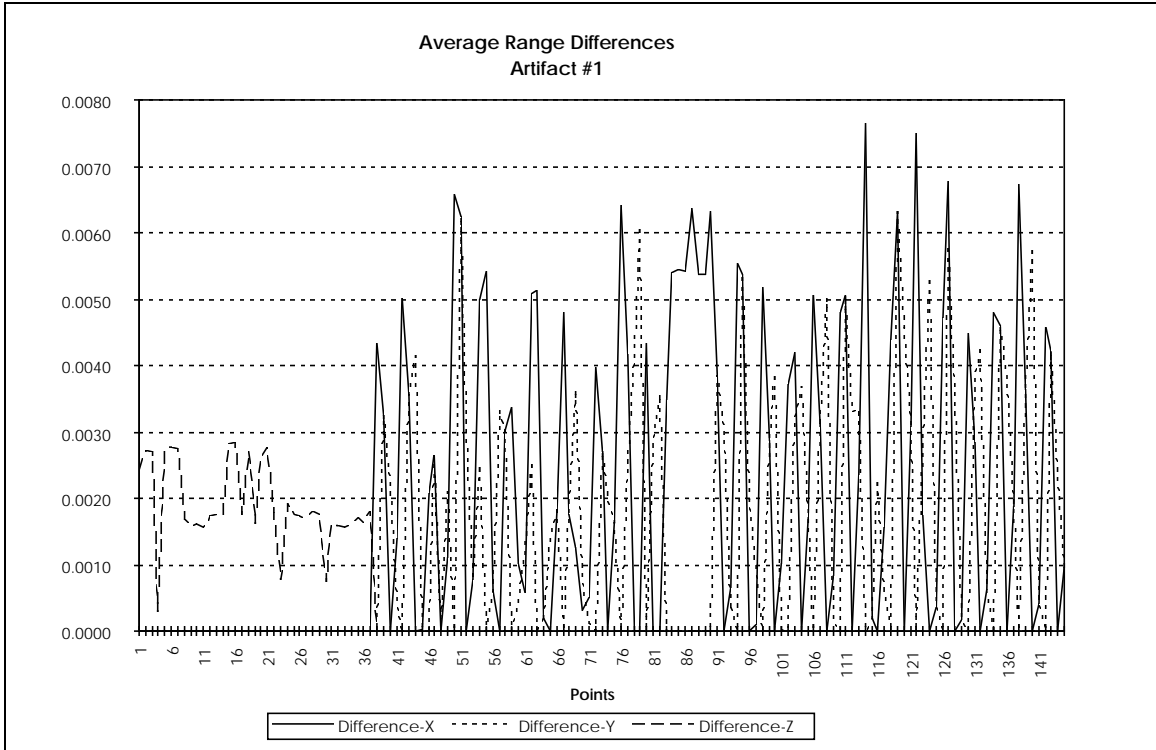
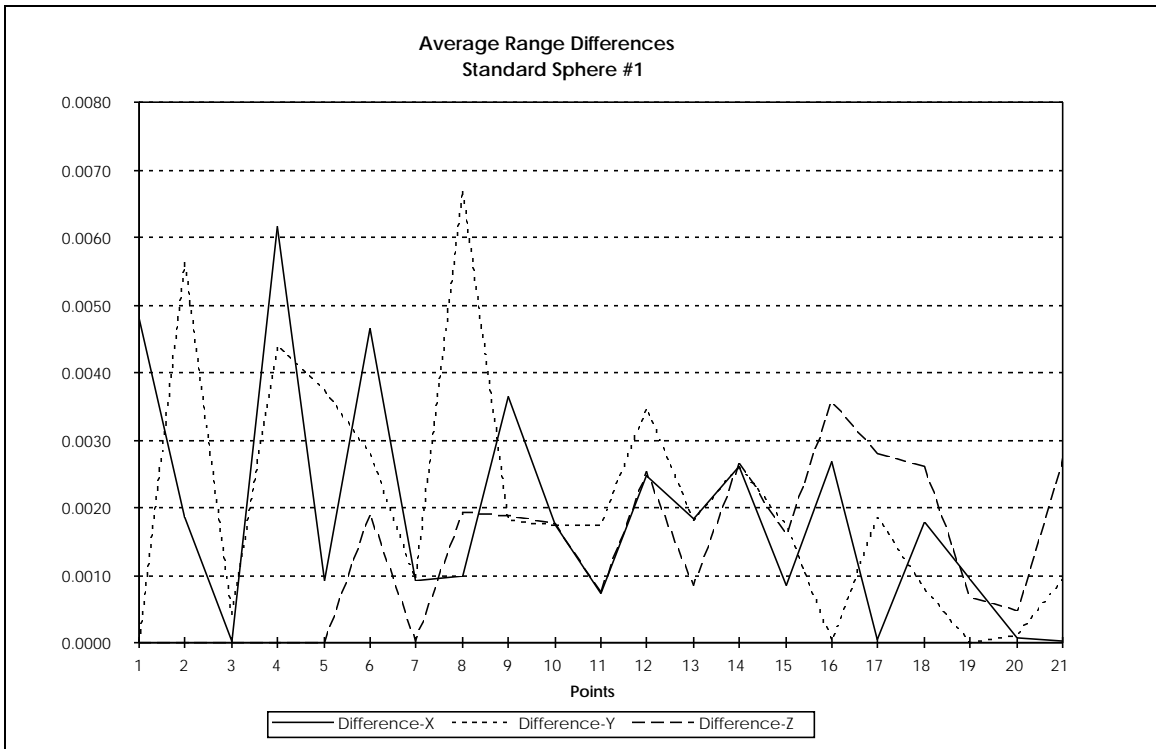


Figure 22. - BostoMatic versus. Zeiss - Artifact Range Difference



**Figure 23. - BostoMatic versus Zeiss - Standard Sphere Range Difference**

For each of the axes, the artifact measurements “track” each other well, i. e., if the BostoMatic measurement range on a point was large, the Zeiss range was also large. This “tracking” indicates the presence of systematic error in one or both of the data sets which could be attributed to mislocation of the part coordinates, probe error, machine error, or the effects of probing direction. The “tracking” is present in measurement ranges of the sphere, but not to the same degree as for the artifact measurements.

The ranges in the X and Y measurements also exhibit the same cyclic patterns for the same reasons that the cyclic patterns occurred for the accuracy analysis. That is, the peaks and valleys occur because of biasing of the X, Y, or Z axes by the CNC program.

Figures 22. and 23. illustrate the differences in range between the BostoMatic and Zeiss in all axes. These measurements were obtained by taking the absolute value of the differences in ranges for all points.

## **10.5 Accuracy and Repeatability Analysis Summary**

To summarize our data analysis, we found that the thermal excursions exhibited a periodic, predictable pattern which we believe could be modeled to correct the measurement error they cause. Further study to determine dependencies between thermal response, machine geometry, part size, and part geometry are recommended. Machine error was also isolated and could be modeled, allowing error correction of the machine tool in a manner similar to that used for CMMs. Statistical analysis of the data could not show that the two machines were measuring identically, but noted the possibility of biases -- alignment, or machine or probe error could be the cause. Measurement accuracy of the machine tool was not comparable to that of the CMM for uncorrected data, but accuracy errors between the two machines were reduced by about 400% when we error-corrected the data using QUALSTAR. Repeatability errors were of the same order of magnitude for both machines. We believe that identifying the errors specific to a machine, creating error maps to correct those errors, and implementing the error maps will provide the same measurement capability for the machine tool as the CMM. OMA will also provide a better understanding of the machining process as a by-product of implementation.

## **11.0 SNL/CA Data Analysis**

Data included analysis of data obtained in the phase one and two OMA study are summarized in the following sections.

## 11.1 Phase One Analysis

The phase one OMA study was divided into two activities. The goal of the first activity was to benchmark and analyze the differences and similarities between CMM and machine tool measurements in raw, uncorrected data. The goal of the second activity was to understand the effect of limited error correction on the accuracy of on-machine inspections versus independent (off-machine) inspections on a second run of artifacts.

### 11.1.1 Benchmark Analysis

The goal of the benchmark data analysis was to:

- Quantify measurement repeatability and uncertainty within a lot of parts manufactured on the same machine (process repeatability),
- Quantify measurement repeatability and uncertainty between multiple inspections of the same part on the same machine (inspection repeatability), and
- Quantify systematic error and uncertainties between OMI and independent inspections.

During machining of the benchmark artifacts, several problems were identified. Initially, the datum -A- surfaces of the artifacts were rough, possibly due to chatter. The feeds and speeds of the part program were modified in an attempt to remove the suspected chatter. After part #SN009 was machined, we determined that the rough datum -A- surface was caused by overmachining in the roughing pass and insufficient cleanup in the finishing pass. The part program was corrected for this problem and a total of 17 artifacts were machined.

Both OMA and CMM data were processed using Geomet inspection software. The output data was formatted as two spreadsheets with a part feature on each row and the inspection results arranged by serial number in the columns. This data was processed to remove some unwanted data points and imported into a Microsoft Excel spreadsheet. Several data were removed (measurements of #SN002A and #SN002B) or combined before processing because of an error in the probing program. Also, the three 4-point intersections used to measure an artifact length were averaged on each part to produce a single measurement of this dimension. The remaining data were plotted with serial number on the X axis and measured value for a single dimension showing both CMM and OMI data on the Y axis.

Several general observations can be made about the plots:

- In many cases the variations track well from CMM to OMI,
- OMI diameter measurements are systematically 0.002" - 0.003" smaller,
- OMI form error measurements are generally two to three times smaller,
- Measurements made with respect to datum -A- are systematically different in #SN002 - #SN009,
- The 3.745" length (Figure 24.) has a smaller systematic error than other measurements,
- The -0.5000" length (Figure 25.) has a 0.008" systematic error from OMI to CMM.

The systematic error between the OMI data and the CMM data appeared to be much larger than expected. We noted that the systematic error could be reduced, but not eliminated by changing the qualification diameter of the probe tip. The probe qualification diameter used by Geomet was 0.0451", but this diameter is unlikely to be correct because the physical size of the probe is 0.0389" and finite stiffness of the probe system requires that qualification diameter is always smaller, not larger. We concluded that an error in the X tool length offset of the probe could cause a one-to-one error in the qualification diameter. It was possible to use the qualification data to correct for the X-axis offset. This new offset was then used to correct the data and reprocess it using Geomet.

The first analysis was performed by comparing the independent inspection data of the lot of parts for trends and repeatability. Trends can be roughly noted by examining the data plots. The examination was inconclusive. Feature sizes were fairly constant throughout the process, except for a possible tendency to get smaller in later artifacts. This was the opposite of what would be expected due to tool wear. The form tolerances also appeared to be constant throughout the lot. In some cases, the forms in the earlier artifacts (#SN001 - #SN008) were larger and erratic, but this may have been due to a problem with the CMM probe documented in the earlier part inspections. The standard deviations of the features are shown in Table 7..

Note that the largest standard deviation of a feature size is approximately 0.0025 inches. This corresponds to a 3-sigma ( $3\sigma$ ) part variation of  $\pm 0.0075$  inches which is a tremendous part size variation within the lot (Column 4, Table 7.). Bolded values designate data where the limits exceed the artifact tolerance (i.e. where the  $C_p$  is less than 1.0). The large variation of artifact feature sizes indicates a lack of repeatability of the machining process.

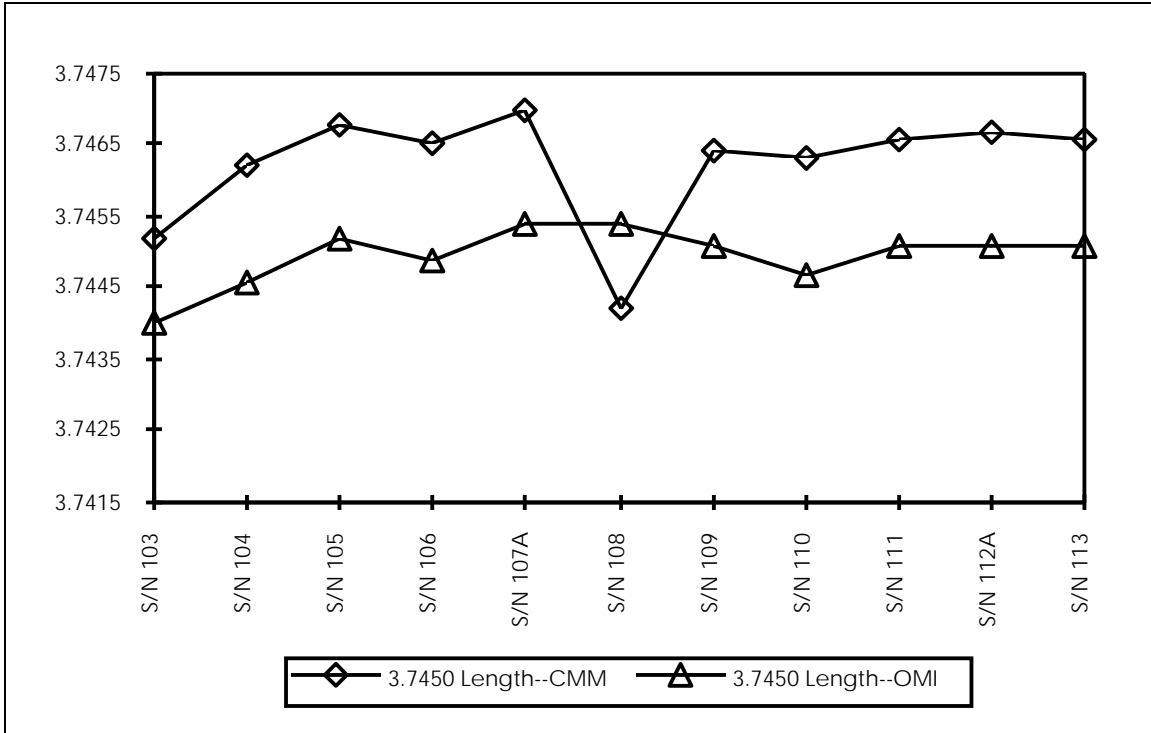


Figure 24. - Plot of 3.745 Inch Linear Dimension

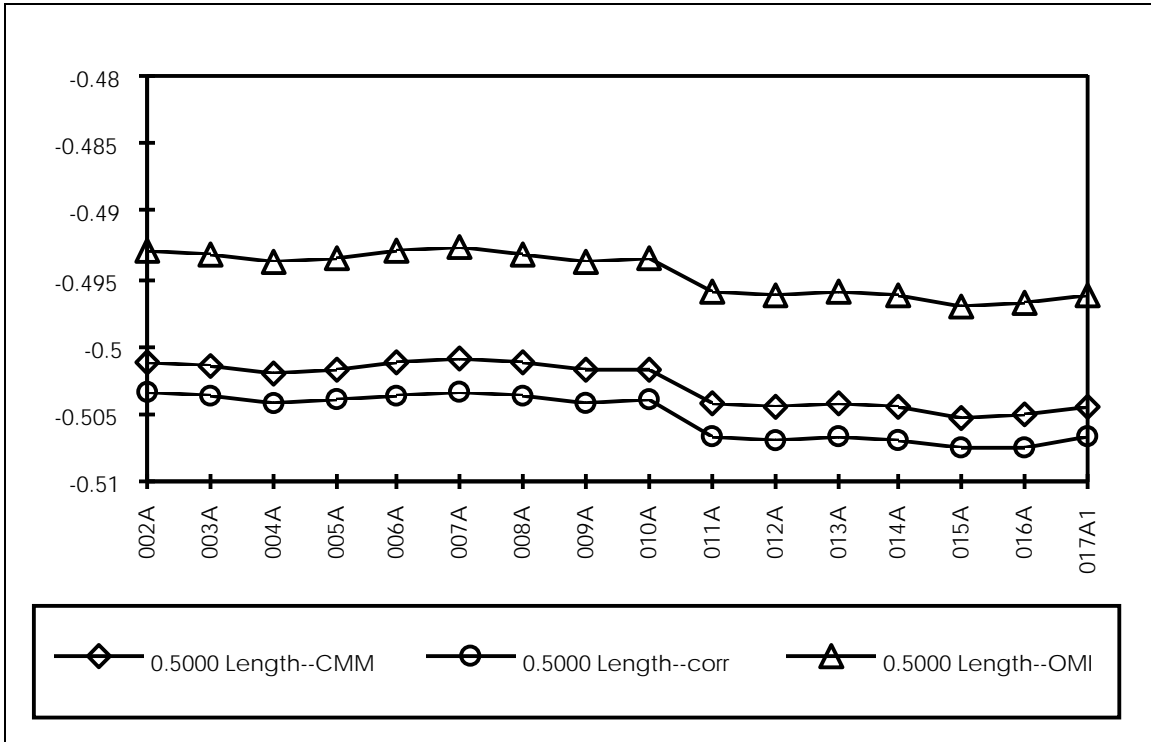


Figure 25. - Plot of -0.500 Inch Linear Dimension



**Table 7. - Standard Deviations - Benchmark CMM Data (inch)**

Feature	Mean - CMM	$\sigma$ - CMM	3 $\sigma$
0.4330 Diameter	0.4308	5.45E-04	$\pm 0.0016$
0.4330 Cylindricity	0.0007	3.22E-04	<b>0.0010</b>
1.6980 Intersection	1.6878	2.58E-03	<b><math>\pm 0.0077</math></b>
49.5 Angle	49.32°	5.78E-02°	$\pm 0.17^\circ$
0.2500 Diameter	0.2477	1.63E-03	$\pm 0.0049$
0.4330 Diameter-End	0.4287	1.53E-03	$\pm 0.0046$
0.4330 Concentricity-End	0.0118	7.92E-03	<b>0.0238</b>
3.7450 Length	3.7436	4.79E-04	$\pm 0.0014$
0.5000 Length	-0.5028	1.66E-03	$\pm 0.0050$
0.9750 Length	0.9753	1.51E-04	$\pm 0.0005$
0.9750 Parallelism	0.0007	1.20E-04	0.0004
1.5000 Diameter	1.4982	4.57E-04	<b><math>\pm 0.0014</math></b>
1.5000 Concentricity	0.0037	1.16E-03	0.0035
1.2500 Radius	1.2491	2.75E-04	$\pm 0.0008$

Several of the artifacts (#SN002, #SN007, #SN013, #SN017) were inspected twice on the machine. Because #SN002 and #SN007 were machined with incorrect datum -A-, they were not considered in the inspection repeatability study. The artifact data from the remaining two pieces were compared to determine the range of measurement values. The inspection repeatability is shown in Table 8..

**Table 8. - Range - Benchmark OMI Data (inch)**

Feature	Range-OMI	Range-OMI-n	Range-CMM
0.4330 Diameter	0.0001	0.0002	0.0001
0.4330 Cylindricity	0.0000	0.0001	0.0002
1.6980 Intersection	0.0007	0.0004	0.0005
49.5 Angle	0.03°	0.03°	0.03°
0.2500 Diameter	0.0001	0.0001	0.0000
0.4330 Diameter-End	0.0003	0.0003	0.0002
0.4330 Concentricity-End	0.0008	0.0006	0.0046
3.7450 Length	0.0003	0.0003	0.0001
0.5000 Length	0.0000	0.0000	0.0002
0.9750 Length	0.0003	0.0003	0.0000
0.9750 Parallelism	0.0003	0.0000	0.0003
1.5000 Diameter	0.0002	0.0002	0.0001
1.5000 Concentricity	0.0004	0.0003	0.0005
1.2500 Radius	0.0002	0.0002	0.0001

The range values were determined by taking the maximum of the range of artifact measurements of #SN013 and #SN017. The range was determined from artifacts measured in the same setup and in most cases, the CMM measurement range was the same or smaller than the OMI measurement range. A notable exception was the ranges associated with form tolerances, which are much larger in the CMM data than the machine data. Once again, these large ranges could be traced to problems with the CMM touch probe. In all cases but one, the measurement repeatability was much better than the process repeatability and was within the expected repeatability of the inspection system.

Identifying discrepancies between OMI and CMM data was performed by comparing and statistically analyzing the measurement data. This analysis was performed twice -- once for the original OMI data, and again for the corrected OMI data. For each data set, the mean of all artifact measurements was calculated. The differences between the OMI means and the CMM data were calculated and a paired t-test was performed to determine if there was any statistically significant agreement between the OMI and CMM data. Finally, an F-test was performed to determine if the OMI and CMM data set variances were similar. The results of these tests are shown in Tables 9. and 10..

In most cases the CMM means were noticeably different from the OMI means; however, the correction of the new OMI data was effective in eliminating some of this discrepancy in the size dimensions. The fourth column represents the results of a paired t-test of the data. The value listed is the probability of the data sets being the same. In the first case, two of the features are significantly similar to a 99% confidence level and none are significantly similar to a 95% confidence level. The correction improved the OMI data to the point where one feature is significantly similar to a 90% confidence level and another similar to a 99% level. In general, the data sets are significantly dissimilar, reflecting a systematic difference between the on-machine measurements and the independent inspection. The last column lists the probability the data sets have similar variances. Dissimilar variances might reflect a difference in process repeatability. These values show that the distributions are mostly similar and that the data correction did little to change the similarities of the distributions.

We implemented the following improvements prior to the start of the second study:

- Implemented a method for insuring proper probe offset settings for the X direction,

- Performed the independent inspection on a CMM equipped with a rotary table, and
- Adjusted the sampling technique so all parts were inspected only once, and some parts, spaced at fixed intervals, were inspected three times for repeatability testing.

**Table 9. - t-test and F-test of Benchmark CMM and OMI Data (inch)**

Feature	Mean-CMM	Mean-OMI	Difference	P(T<=t)	P(F<=f)
0.4330 Diameter	0.4308	0.4288	0.002	1.26E-11	<b>0.442</b>
0.4330 Cylindricity	0.0007	0.0003	0.0004	4.28E-05	7.13E-05
1.6980 Intersection	1.6878	1.6967	-0.0089	2.65E-10	<b>0.488</b>
49.5 Angle	49.32°	49.21°	0.11°	<b>0.0221</b>	9.01E-08
0.2500 Diameter	0.2477	0.2454	0.0023	2.67E-06	<b>0.314</b>
0.4330 Diameter-End	0.4287	0.4272	0.0015	2.06E-03	4.69E-04
0.4330 Concentricity-End	0.0118	0.0066	0.0052	<b>0.0123</b>	1.30E-03
3.7450 Length	3.7436	3.7433	0.0003	3.79E-05	<b>0.481</b>
0.5000 Length	-0.5028	-0.4946	-0.0082	4.16E-33	<b>0.487</b>
0.9750 Length	0.9753	0.9749	0.0004	9.09E-05	<b>0.136</b>
0.9750 Parallelism	0.0007	0.0005	0.0002	5.90E-04	<b>0.0249</b>
1.5000 Diameter	1.4982	1.4964	0.0018	7.89E-12	<b>0.470</b>
1.5000 Concentricity	0.0037	0.0012	0.0025	1.36E-07	<b>0.0194</b>
1.2500 Radius	1.2491	1.2485	0.0006	8.71E-12	<b>0.365</b>

**Table 10. - t-test and F-test of Benchmark CMM and Corrected OMI Data (inch)**

Feature	Mean-CMM	Mean-OMI-n	Difference	P(T<=t)	P(F<=f)
0.4330 Diameter	0.4308	0.4298	0.001	1.58E-07	<b>0.434</b>
0.4330 Cylindricity	0.0007	0.0003	0.0004	2.36E-04	2.91E-07
1.6980 Intersection	1.6878	1.6914	-0.0036	8.30E-08	<b>0.497</b>
49.5 Angle	49.32°	49.21°	0.11°	<b>0.0186</b>	1.61E-07
0.2500 Diameter	0.2477	0.2464	0.0013	9.44E-04	<b>0.308</b>
0.4330 Diameter-End	0.4287	0.4282	0.0005	<b>0.207</b>	4.50E-04
0.4330 Concentricity-End	0.0118	0.0063	0.0055	7.99E-03	1.28E-03
3.7450 Length	3.7436	3.7433	0.0003	3.79E-05	<b>0.481</b>
0.5000 Length	-0.5028	-0.5052	0.0024	4.86E-25	<b>0.487</b>
0.9750 Length	0.9753	0.9749	0.0004	9.09E-05	<b>0.136</b>
0.9750 Parallelism	0.0007	0.0005	0.0002	5.90E-04	<b>0.0249</b>
1.5000 Diameter	1.4982	1.4974	0.0008	4.59E-07	<b>0.470</b>
1.5000 Concentricity	0.0037	0.0012	0.0025	1.05E-07	3.93E-03
1.2500 Radius	1.2491	1.2482	0.0009	1.37E-14	<b>0.373</b>

### 11.1.2 Error-Corrected Analysis

The goals of the error-correction data analysis were the same as in the benchmark study. To reiterate, the goals were to quantify repeatability and uncertainty on a lot manufactured on the same machine and

between multiple inspections, and to quantify systematic error and uncertainties between OMI and CMM measurements.

The probe pretravel variation data was separated into two groups -- the 5 data sets recorded at 0° spindle locations and the 5 sets recorded at 90° spindle locations. Each data set was processed using Geomet to compute the sphere center in X and Z. The sphere center locations were then subtracted from each data point in the set to correct for the pretravel variation. Each group of data was then averaged and the averaged results are shown in Figure 26..

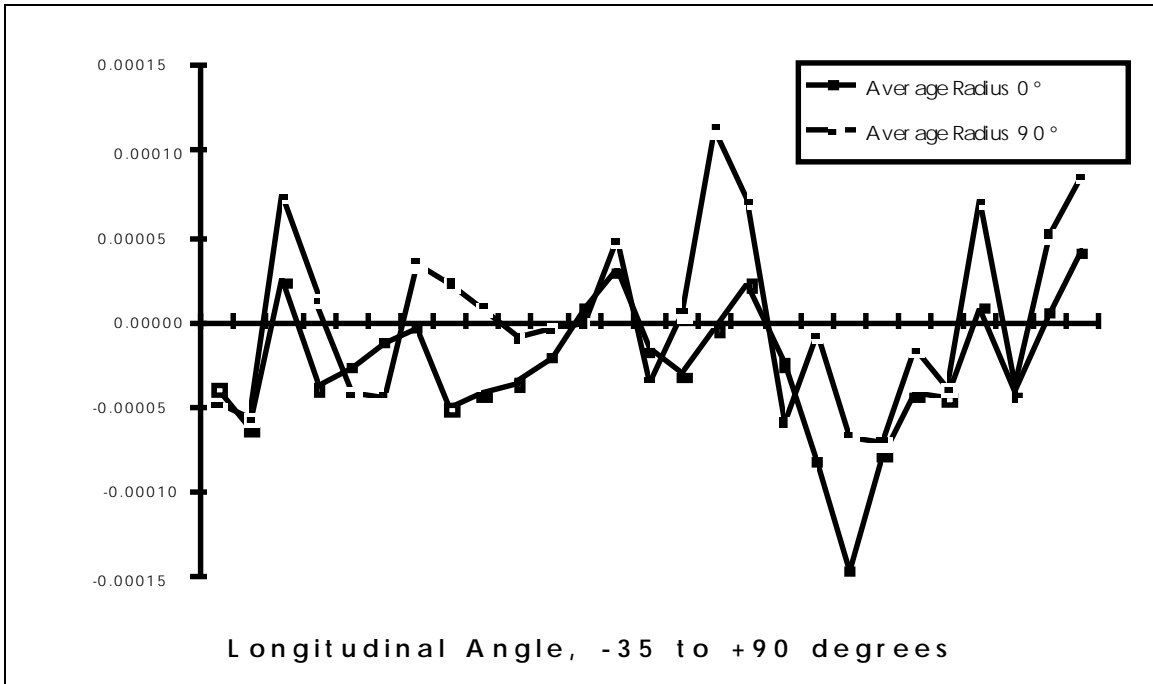


**Figure 26. - Probe Pretravel Variation at 0° and 90° vs. Approach Angle**

Figure 26. illustrates that there does not appear to be much repeatable systematic pretravel error. The spread between the two data sets shown in Table 11. reinforces the non-repeatability observation. Figure 26. and Table 11. also illustrate that the spread within the two groups of data is significantly larger than the spread between the two groups of data suggesting that the data is too noisy to accurately correct the probe pretravel variation.

**Table 11. - Differences at 0° and 90° - Probe Pretravel Variation**

Average difference of averaged data	28 x 10 <sup>-6</sup> inch
Maximum difference of averaged data	117 x 10 <sup>-6</sup> inch
Standard deviation of 5 sets of 0 degree data	78 x 10 <sup>-6</sup> inch

Standard deviation of 5 sets of 90 degree data	$71 \times 10^{-6}$ inch
--	--------------------------

To prove this, the 0° data set was used to attempt to correct the 90° degree data set. At each point along the longitudinal axis, the average of the 0° data set was subtracted from the average of the 90° data set. In an ideal situation, the resulting corrected value should be zero at all points along the axis. The deviation from zero was measured by taking the root sum of the squares of the deviations of each point from zero. The results are shown in Table 12..

**Table 12 - Root Sum Squares of Differences at 0° and 90° - Probe Pretravel Variation**

RSS of 90° average data before correction	265 x 10 <sup>-6</sup> inch
RSS of 90° average data after correction	238 x 10 <sup>-6</sup> inch
Percent improvement	10%

We determined that the resulting improvement of 10% was insignificant, so no probe pretravel variation correction was performed. The probe was set in the X direction using the previously described procedure with a resulting probe set accuracy of less than 0.001".

Two minor machining problems occurred during the error correction study. First, one of the probing routines had to be corrected because of changes made by another lathe user. Second, artifacts #SN102 - #SN113 were turned from smaller stock, so the soft-jaws also had to be turned down for artifacts #SN101 and #SN102. As a result, #SN101 and #SN102 were not considered in the data analysis. We suspected that the tool offsets were wrong, and after turning #SN103, the control showed a turret fault. The lathe was restarted and the problem did not recur.

The remaining CMM and OMI data were plotted as in the benchmark study and the following observations were made about the plots:

- The variations track well from CMM to OMI,
- The OMI diameters are fairly constant throughout. The CMM measurements show a distinctive shift to better agreement with lathe measurements at #SN108, corresponding to the fact that it was turned on a different day,
- OMI diameter measurements are systematically 0.001" smaller,
- The 0.5000" length tracks extremely well from OMI to CMM,
- All features measured on the CMM with respect to datum -A- for #SN108 are outliers possibly because #SN108 was a robotic cell test part,

- OMI length measurements are systematically 0.001" to 0.002" smaller than CMM measurements, and
- Form error measurements between the lathe and the CMM are fairly similar with the exception of the 1.5000" concentricity.

The first analysis was performed by examining the plotted CMM measurements for trends and repeatability. With the exception of the shift in measured diameters beginning with #SN108 noted above, there does not appear to be any trend behavior. The form tolerances also appear to be constant throughout the lot. The standard deviations of the features are shown in Table 13. along with the corresponding data from the benchmark pilot. It should be noted that the parts produced in the correction pilot are much more consistent.

**Table 13. - Comparison of Standard Deviations in Benchmark and Corrected CMM Data (inch)**

Feature	Mean-CMM, Benchmark	Mean-CMM, Corrected	3 sigma, Benchmark	3 sigma, Corrected
0.4330 Diameter	0.4308	0.4352	±0.0016	±0.0013
0.4330 Cylindricity	0.0007	0.0003	<b>0.0010</b>	0.0002
1.6980 Intersection	1.6878	1.6876	<b>±0.0077</b>	±0.0023
49.5 Angle	49.32°	49.03°	±0.17°	±0.09°
0.2500 Diameter	0.2477	0.2510	±0.0049	±0.0021
0.4330 Diameter-End	0.4287	0.4341	±0.0046	±0.0017
0.4330 Concentricity-End	0.0118	0.0029	<b>0.0238</b>	<b>0.0056</b>
3.7450 Length	3.7436	3.7464	±0.0014	±0.0015
0.5000 Length	-0.5028	-0.5077	±0.0050	±0.0022
0.9750 Length	0.9753	0.9769	±0.0005	±0.0003
0.9750 Parallelism	0.0007	0.0005	0.0004	0.0004
1.5000 Diameter	1.4982	1.5017	<b>±0.0014</b>	<b>±0.0013</b>
1.5000 Concentricity	0.0037	0.0025	0.0035	0.0012
1.2500 Radius	1.2491	1.2510	±0.0008	±0.0006

Note that the worst 3-sigma ( $3\sigma$ ) part variation for a corrected size measurement is ±0.0023" in Table 13.. This variation is significantly smaller than the benchmark results shown in Table 7., but still significant compared to the artifact tolerances. The 3-sigma values are bold where the limits exceed the tolerance (i.e. where the Cp is smaller than 1.0). The variation of part feature sizes indicates a lack of repeatability of the machining process.

Several of the parts (#SN102, #SN107, and #SN112) were inspected three times on the machine. Because #SN102 was made with incorrect datum -

A-, it was not considered in the inspection repeatability study. The artifact data from the remaining two pieces were compared to determine the range of measurement values. The inspection repeatability is shown in Table 14. along with data from the benchmark pilot for comparison.

**Table 14. - Comparison of Ranges in  
Benchmark and Corrected OMI Data (inch)**

Feature	Range-OMI, Benchmark	Range-OMI, Corrected	Range-CMM, Benchmark	Range-CMM, Corrected
0.4330 Diameter	0.0001	0.0008	0.0001	0.0000
0.4330 Cylindricity	0.0000	0.0001	0.0002	0.0001
1.6980 Intersection	0.0007	0.0012	0.0005	0.0003
49.5 Angle	0.03°	0.07°	0.03°	0.07°
0.2500 Diameter	0.0001	0.0008	0.0000	0.0000
0.4330 Diameter-End	0.0003	0.0006	0.0002	0.0001
0.4330 Concentricity-End	0.0008	0.0009	0.0046	0.0032
3.7450 Length	0.0003	0.0005	0.0001	0.0001
0.5000 Length	0.0000	0.0000	0.0002	0.0000
0.9750 Length	0.0003	0.0006	0.0000	0.0001
0.9750 Parallelism	0.0003	0.0001	0.0003	0.0001
1.5000 Diameter	0.0002	0.0007	0.0001	0.0001
1.5000 Concentricity	0.0004	0.0005	0.0005	0.0008
1.2500 Radius	0.0002	0.0003	0.0001	0.0001

The range values were determined by taking the maximum of the range of artifact measurements of #SN107 and #SN112. In each case, the range was determined from artifacts measured in the same setup. In most cases, the range of CMM measurements was the same or less than the range of the machine tool measurement. A notable exception was the ranges of concentricity, which were much larger in the CMM than on the machine tool. This difference in concentricity range may be due to the CMM procedure of measuring all features from one side. This method of measurement may bias the center locations of cylinders on the artifact. In all other cases, the inspection repeatability for artifacts was much better than the machining process repeatability and was within the expected repeatability of the inspection system.

We identified discrepancies between OMI and CMM data by comparing and statistically analyzing the inspection data. The average value for all features was calculated and then the differences between the OMI and CMM averages were calculated. Next, a paired t-test was performed for each feature to determine if there was statistically significant agreement between the OMI and CMM data. Finally, an F-test was performed to determine if the variances of the OMI and CMM data sets were similar. The results of these paired t-tests and F-tests are shown in Table 15..

**Table 15. - t-test and F-test of CMM and Corrected OMI Data (inch)**

Feature	Mean-CMM	Mean-OMI	Difference	P(T<=t)	P(F<=f)
0.4330 Diameter	0.4352	0.4345	0.0007	1.31E-03	1.77E-03
0.4330 Cylindricity	0.0003	0.0002	0.0001	1.10E-03	<b>0.0184</b>
1.6980 Intersection	1.6876	1.6888	-0.0012	<b>0.2542</b>	2.47E-04
49.5 Angle	49.03°	49.14°	-0.11°	1.21E-06	<b>0.245</b>
0.2500 Diameter	0.2510	0.2498	0.0012	4.90E-05	<b>0.0131</b>
0.4330 Diameter-End	0.4341	0.4328	0.0013	1.94E-05	3.27E-04
0.4330 Concentricity-End	0.0029	0.0027	0.0002	<b>0.8347</b>	<b>0.318</b>
3.7450 Length	3.7464	3.7449	0.0015	1.08E-10	<b>0.272</b>
0.5000 Length	-0.5077	-0.5075	-0.0002	2.03E-04	<b>0.394</b>
0.9750 Length	0.9769	0.9750	0.0019	9.18E-10	<b>0.0400</b>
0.9750 Parallelism	0.0005	0.0005	0.0000	<b>1.0000</b>	6.77E-03
1.5000 Diameter	1.5017	1.5010	0.0007	2.41E-03	2.67E-03
1.5000 Concentricity	0.0025	0.0009	0.0016	1.79E-05	<b>0.401</b>
1.2500 Radius	1.2510	1.2504	0.0006	6.71E-05	<b>0.194</b>

In most cases, the CMM averages were noticeably different from those of the machine tool. The values listed in column five of Table 15. are the results of paired t-tests of the data which represent the probability that the data sets are identical. Three of the features (bolded numbers) were significantly similar with a very high level of confidence. The rest were significantly dissimilar, reflecting a systematic difference between the on-machine measurements and the independent (CMM) inspection. Note that the results of the t-test are generally better than those of the benchmark study (column five, Table 9.). The t-test improvement may be due to the linear accuracy correction that was implemented in the error correction analysis. The last column in Table 15. lists the probability the data sets have similar variances. Dissimilar variances might reflect a difference in process repeatability. The bolded values show that the distributions were mostly similar and there did not appear to be a significant change in the F-test results of the benchmark and corrected data studies.

A comparison of the t-test and F-test results for both the benchmark and corrected data is shown in Table 16..

**Table 16. - Comparison of t-test and F-test  
in Benchmark and Corrected OMI Data (inch)**

Feature	P(T<=t), Benchmark	P(T<=t), Corrected	P(F<=f), Benchmark	P(F<=f), Corrected
0.4330 Diameter	1.58E-07	1.31E-03	<b>0.434</b>	1.77E-03
0.4330 Cylindricity	2.36E-04	1.10E-03	2.91E-07	<b>0.0184</b>
1.6980 Intersection	8.30E-08	<b>0.2542</b>	<b>0.497</b>	2.47E-04
49.5 Angle	<b>0.0186</b>	1.21E-06	1.61E-07	<b>0.245</b>
0.2500 Diameter	9.44E-04	4.90E-05	<b>0.308</b>	<b>0.0131</b>
0.4330 Diameter-End	<b>0.207</b>	1.94E-05	4.50E-04	3.27E-04
0.4330 Concentricity-End	7.99E-03	<b>0.8347</b>	1.28E-03	<b>0.318</b>
3.7450 Length	3.79E-05	1.08E-10	<b>0.481</b>	<b>0.272</b>
0.5000 Length	4.86E-25	2.03E-04	<b>0.487</b>	<b>0.394</b>
0.9750 Length	9.09E-05	9.18E-10	<b>0.136</b>	<b>0.0400</b>
0.9750 Parallelism	5.90E-04	<b>1.0000</b>	<b>0.0249</b>	6.77E-03
1.5000 Diameter	4.59E-07	2.41E-03	<b>0.470</b>	2.67E-03
1.5000 Concentricity	1.05E-07	1.79E-05	3.93E-03	<b>0.401</b>
1.2500 Radius	1.37E-14	6.71E-05	<b>0.373</b>	<b>0.194</b>

### 11.1.3 Phase One Analysis Summary

Based on the results of the SNL/CA benchmark study, the following observations and conclusions about OMA on the lathe can be made:

- It was difficult to reach all features of a turned component without an indexable probe head,
- The experimental setup for the benchmark study was sufficient,
- OMI currently cannot effectively detect form errors,
- The machining process spread was outside the tolerance band for many features and close to the tolerance band for most others,
- The process spread was not centered about the target feature size,
- The measurement repeatability was a small fraction of the process repeatability,
- CMM repeatability was better than the OMI repeatability for most features, and
- OMI values were systematically different from independent inspection values to a statistical confidence of 99% for most features.

Based on the results of the SNL/CA error correction study, the following observations and conclusions about OMA on the lathe can be made:

- The study of probe pretravel variation was inconclusive,
- A method to correct for probe-setting errors in the X direction was successfully implemented,
- The machining process spread still comprised a large portion of the tolerance band,
- OMI measurement repeatability was a significant portion of the tolerance band,
- The process spread was not centered about the target feature size,
- For most features, the CMM repeatability was better than OMI repeatability,
- The agreement between OMI and CMM measurements for feature size was much better than in the benchmark study,
- Systematic differences still exist between OMI and CMM measurements, and
- The OMA artifact can be damaged by handling in the Integrated Manufacturing Technologies Laboratory (IMTL) cell.

Furthermore, the following improvements are recommended before further error correction studies on the lathe begin:

- Check the toolsetting accuracy before using it to set tools,
- Perform a systematic study of probe pretravel variation,
- Determine the accuracy of the software probe-setting method in the X direction,
- Compute form errors for more of the artifact features to obtain more data,
- Evaluate the CMM measurement accuracy, and
- Perform the independent inspection on a CMM equipped with a rotary table.

## 11.2 Phase Two Graphic Visualization Demonstration

One commercial three-dimensional visualization software package that we considered for advanced OMA was AVS/Express because it was more flexible, extensible, easier to use, and offers more convenient features than other visualization systems. AVS/Express also offers unified two- or three-dimensional pipelines to support integrated rendering and annotation of images, two- or three-dimensional objects and volumes in the same coordinate system. AVS/Express operates on SGI, Sun, and HP workstations as well as PC desktop computer systems. AVS/Express also

accepts data through network sockets to allow near real-time data display. The system generates VRMLs. Using the developers software, a single graphical user interface application can be developed and then run on an unlimited number of platforms.

The sensor data collected from the Haas mill was used to demonstrate the capabilities of the AVS/Express software. Fourteen in-process sensor measurements -- three-dimensional tool force, vibration, acoustic emissions, and torque were made on the artifact. The image shown in Figure 27. below illustrates the capability of AVS/Express to visualize three-dimensional, color-mapped force data along the tool path as the artifact is machined.

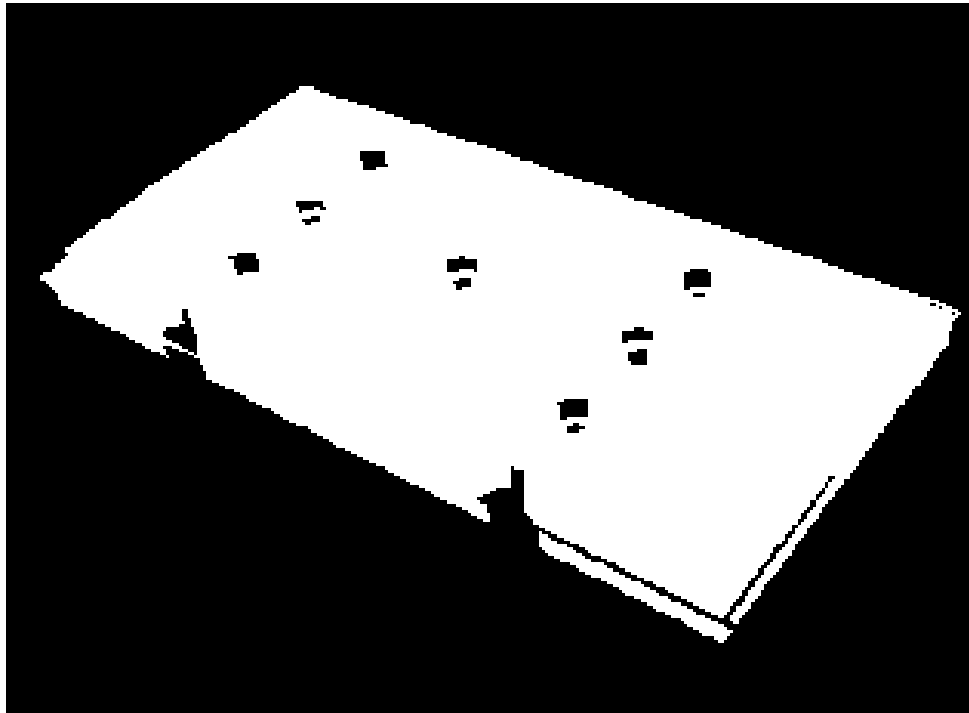


**Figure 27. - AVS/Express Force Visualization on Phase Two Artifact**

AVS/Express allows the plotting of multiple data sets on the artifact model simultaneously. In addition, various sensor information can be evaluated by the machinist as the processing occurs to determine whether additional testing of the part is necessary in order to accept it. A useful example of the machining process visualization is to plot tool force data to detect inconsistency in the machining forces. If inconsistencies in the forces are present, the machinist may decide that further dimensional verification of the part is required in order to determine if the part is acceptable. Various data visualization techniques, for example overlaid

bar charts along tool paths, can be used to give the machinist a more complete understanding of the process and the data.

## **12.0 SNL/NM OMA Issues**

This section updates the status of problems/issues encountered by the SNL/NM team, and lessons learned prior to the beginning of the LDRD, and during FY95 and FY96. Some of these problems/issues were due to a lack of knowledge of the hardware and software interactions.

### **12.1 Probing Strategies**

Due to the lack of consensus regarding probing strategy, and time and budget constraints, we decided that continued development of probing strategies were outside the scope of the LDRD. Valid probing strategy must address surface finish, deviation from perfect geometric form, the optimum number of points, the point location, point density, and methods of manufacturing because these all affect the accuracy and reliability of the measurement. Other factors related to probing strategies are the algorithms used to calculate size and location of part geometry such as least-squares, maximum inscribed circles, or minimum circumscribed circles. The Consortium for Advanced Manufacturing-International (CAM-I) is working on generic probing strategies that address many of these issues.

### **12.2 Probe (Sensor) Technologies**

The type of probe or sensor used for OMA impacts the accuracy and reliability of the data. The amount of data the probe gathers in a set time period is advantageous only if the data is accurate. Probes that gather discrete data points are limited as to the amount of data that they can acquire at a time, but they are usually more accurate than probes that can scan more data in a shorter time.

Accuracy and repeatability and the probe technologies employed affect the accuracy and reliability of the data. For example, mechanical probes exhibit probe lobing errors, optical probes are sensitive to the surface reflectivity of the part being measured, and capacitance probes are affected by the type of material being probed or the coolants used in the machining process. Robust probe designs provide survivability in machining environments where vibration, coolant, chips, and temperature extremes are present.

Detailed sensor information can be found in SAND95-3061, "Laboratory Directed Research and Development - Interim Report - Intelligent Tools for On-Machine Acceptance of Precision Machined Components" <sup>1</sup>.

### **12.3 Part Location on Machine**

To machine the artifact, the collet holding the unmachined artifact blank must be manually located coaxial to the BostoMatic spindle.

Misalignment between the spindle and the collet results in misalignment of any machined features which results in a data shift. Additionally, when the tool is changed out of the spindle to accept the Renishaw probe, a misalignment between the probe stylus and artifact may occur. The QUALSTAR best-fit data analysis detects the shift because it fits data to the part model which is independent of the machine or CMM coordinate system.

### **12.4 Probe Alignment and Probe-to-Part Coordinate System**

The Zeiss uses its measurement software to probe a calibration standard and determine the probe stylus diameter. It also probes the artifact and establishes the coordinate system for the artifact and maintains the relationship of the probe stylus location to the artifact location. It has this capability even with unusual probe configurations such as star cluster or elbow-shaped probes. The BostoMatic cannot determine the relationship and has no measurement software to process data to determine feature size or location as the Zeiss does. The BostoMatic can only collect the artifact data. Any data analysis must be done with software such as Excel or QUALSTAR.

This inability to process data to establish probe locations or part coordinate systems affects the BostoMatic's ability to establish a coaxial relationship between the spindle and the probe stylus. The coaxial relationship must be established by indicating and adjusting the probe stylus manually while the BostoMatic spindle is turned until no runout between the probe stylus and spindle exists. Any misalignment however slight, has the potential to affect the part measurements. This is a problem that could be corrected by installing measurement software on the BostoMatic so that it is capable of determining the probe/spindle relationship. QUALSTAR best-fit analysis detects these misalignments because it shows as a shift of the artifact features in relationship to the probed points.

### **12.5 Data Mismatch**

The Silma probe path generation software resolved many of the data point mismatch problems encountered during the first half of the LDRD so

that the probe paths for both machines were identical. The BostoMatic probe radius compensation is still not functional so the data we acquired was still ball-center data, but it was possible to compensate the Zeiss for a "zero" probe radius allowing us to compare point-to-point data.

## **12.6 Approach/Retract Speed Variation**

We determined that a slower retract speed for the BostoMatic did improve the measurement repeatability, although there appears to be no effect on the accuracy of the measurement. Further study to determine the effect of overtravel and opposite probing directions (between the BostoMatic and the Zeiss) is necessary.

## **12.7 QUALSTAR**

The ACCORD agreement required that the NWC standardize the software used to design and manufacture weapons hardware. The incompatibilities between QUALSTAR and ProEngineer discussed in the interim report <sup>1</sup> were caused in part by our desire to use the ACCORD software. These incompatibilities may not exist for other CAD software making use of two dimensional IGES files (ProEngineer exports three-dimensional IGES files). AS-FM&T has obtained the funding to continue development of the interface that converts ProEngineer files into the preferred QUALSTAR IGES format. As of this writing, QUALSTAR is still not capable of creating part models with trim surfaces (surfaces that intersect at right angles).

In our opinion, QUALSTAR is still the best choice for data analysis because it is ANSI Y14.5 compatible, it allows us to evaluate data in close to real time with a clear graphical representation of the artifact condition, it performs a best-fit of the data, and it performs statistical analysis. As other data analysis software with QUALSTAR's capabilities become available, we hope to evaluate them for OMA purposes.

## **13.0 Future OMA Activities**

The following sections are short descriptions of the partners or contacts with whom we have discussed OMA. Particular OMA interests and any resulting activities are described briefly below.

### **13.1 OMA Activities at AS-FM&T**

Process Development Program (PDP) guidance has been written to pursue OMA and evaluation of soft functional gaging at AS-FM&T. As mentioned above, staff at AS-FM&T are continuing development of the ProEngineer/QUALSTAR interface. Because LDRD funding expired at the

end of FY96, OMA technology is being transferred and will be implemented and qualified at AS-FM&T in FY97 for use on War Reserve (WR) product. AS-FM&T plans to implement OMA on a Monarch Vertical Milling Center.

## 13.2 OMA Contacts

SNL/NM and SNL/CA held a jointly sponsored OMA demonstration in September of 1996 to show the technology to industry and determine the level of interest in joint development. The industries that have visited Sandia include B. F. Goodrich, Boeing, Caterpillar, Eastman Kodak, Eaton Corporation, General Electric, United Technologies-Sikorsky and Pratt & Whitney divisions, and Vickers. Manufacturers of machine tools, probes, and machine tool maintenance equipment include Cincinnati Milacron, Giddings and Lewis, Extrude Hone, and Automated Precision, Inc.. Interested academia include New Mexico State University and University of Missouri, Rolla. The interest shown by attendees of the September demonstration has initiated plans for a second demonstration/workshop to be held at SNL/NM in FY97.

## 13.3 Further Development of OMA

Figure 28. illustrates SNL/NM's vision for OMA. Functional OMA modules, modules that are under development, or modules needing development are shown. From this illustration, it is quite evident that much work remains to be done, with much of this work applicable to both CMM and OMA qualification activities.

Briefly, beginning from the CAD workstation, we would like to integrate the following activities. The part model will be created in ProEngineer and this information input to both a decision support system for Process Characterization Methodology (PCM) and a smart fixture design assistant. PCM provides a means to identify critical processes and implement the necessary controls to prevent product faults from occurring in critical processes. Our goal is to implement PCM as an intelligent Decision Support System to assist designers in choosing materials, product features, and processes based on historical design information on similar products. Another SNL/NM LDRD has developed an intelligent decision support system to design fixtures that will provide stable and secure support to minimize part distortion, and the number of required fixtures and setups. The CAD station can be used for fixture and part design and to simulate the fit between part and fixture. After design, the part model will be input to the ProEngineer/QUALSTAR interface to design a soft gage and prepare for data evaluation and part acceptance. The model will also be used to design part probing paths. Optimally, a formal probing strategy based on the manufacturing methods, geometry type, tolerance, and degree of confidence required by the part application would be used to design the probing paths.

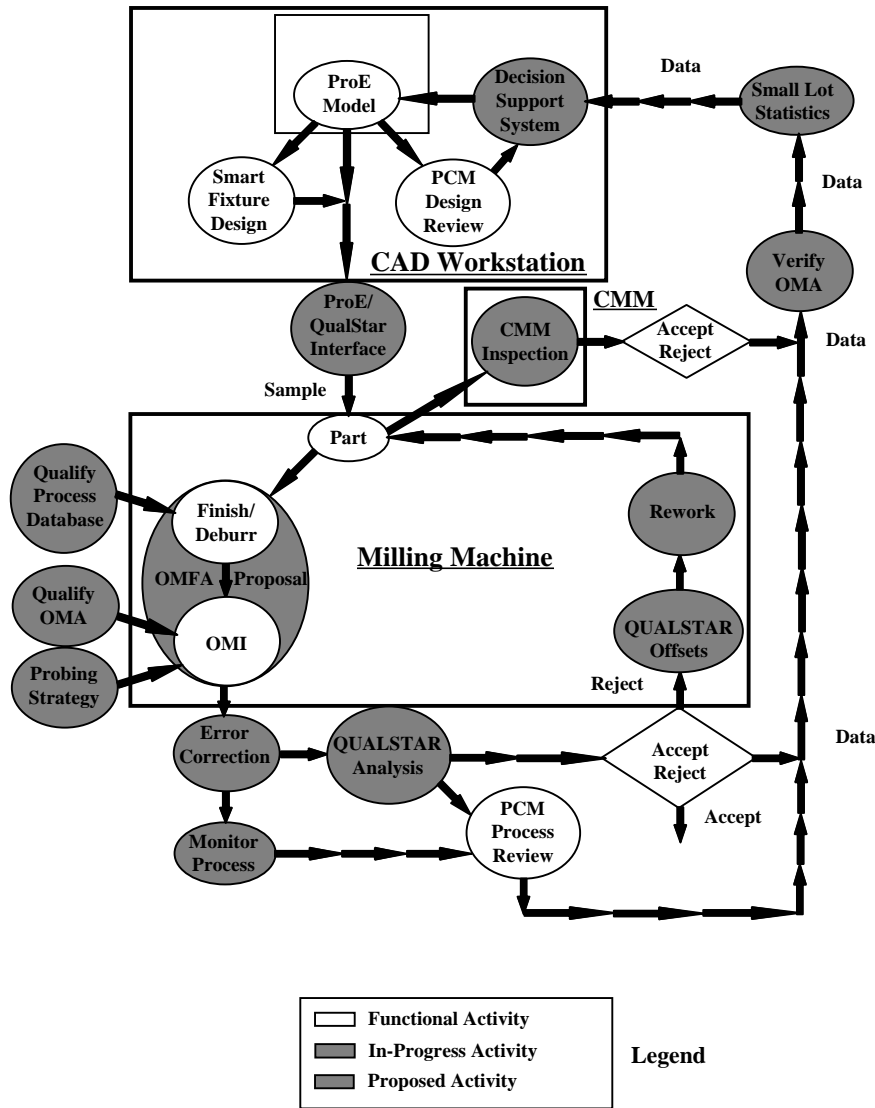


Figure 28. - Vision for Future OMA Development

The model is then exported to the machine tool where the machining program can be written. The part is machined and inspected and the data is exported to QUALSTAR for data analysis and part disposition. The part disposition could be acceptance, rework, a finish cut, or finishing (deburring). If the part is acceptable, QUALSTAR can generate the acceptance report. If the part requires a finish cut, QUALSTAR can generate part offsets which can be used to adjust part location on the machine. If the part requires rework, the part can be re- fixtured, probed, the data run through QUALSTAR for a best fit analysis, and the part offsets used to establish a part coordinate system for rework.

With a finished or reworked part, some type of deburring is usually necessary. Another LDRD project developed a database and programming assistant to predict burr characteristics based on the machining and material parameters. The database uses the part model, and machining and material parameters to predict the size of burrs and where they will occur on the part. The programming assistant creates paths to drive the machine tool over areas where the burrs occur to remove them. If the part has not been removed, the part coordinate system is intact and deburring occurs next. If the part has been reworked, the part location and coordinate system has already been established by probe data and QUALSTAR offsets, so deburring can occur next.

Error maps will also be created to correct for probe error, machine error, and optimally, thermal error. Data obtained by the OMI can also be used to monitor the process and can be input to a database used to generate small lot statistics for the product. Small lot statistics are useful in high consequence applications, such as nuclear weapons, where the product is produced in small quantities, but requires a high functional reliability. The process data can also be input to the PCM database to maintain a historical record linking materials, process information such as burr size or machining time, and statistical data about the machining process for similar future applications. A sample of parts may also be run under the CMM to verify OMI measurements and part disposition decisions. Thus, the integration of all OMA functionalities is driven by the part model and design intent.

## 14.0 Figures and Tables

Figure 1. - Comparison of Conventional Product Realization to OMA .....	5
Figure 2. - Relative Interest in OMA of Potential End Users.....	12
Figure 3. - SNL/NM OMA Artifact and Probed Point Location.....	15
Figure 4. - SNL/CA OMA Artifact .....	15
Figure 5. - Probe Setting in X Direction - Spindle Position = 0° .....	21
Figure 6. - Probe Setting in X Direction - Spindle Position = 180°.....	22
Figure 7. - OMA Cost Savings.....	25
Figure 8. - BostoMatic Thermal Response - Six Locations .....	26
Figure 9. - Raw X Axis Data.....	30
Figure 10. - Steady-State Error Correction of X Axis Data .....	30
Figure 11. - Steady-State Error Correction and Least Squares Fit .....	
Polynomial Equation of X Axis Data .....	31
Figure 12. - Fourier Series Period Error Modeling of X Axis Periodic Data.....	32
Figure 13. - BostoMatic Accuracy - Comparison of Average Uncorrected Artifact Values.....	37
Figure 14. - BostoMatic Accuracy - Comparison of Average Corrected Artifact Values.....	38
Figure 15. - BostoMatic Accuracy - Comparison of Average Corrected Standard Sphere Values.....	39
Figure 16. - BostoMatic vs. Zeiss - X Axis Range on Artifact .....	42
Figure 17. - BostoMatic vs. Zeiss - X Axis Range on Standard Sphere .....	42
Figure 18. - BostoMatic vs. Zeiss - Y Axis Range on Artifact .....	43
Figure 19. - BostoMatic vs. Zeiss - Y Axis Range on Standard Sphere .....	43
Figure 20. - BostoMatic vs. Zeiss - Z Axis Range on Artifact.....	44
Figure 21. - BostoMatic vs. Zeiss - Z Axis Range on Standard Sphere.....	44
Figure 22. - BostoMatic vs. Zeiss - Artifact Range Difference .....	45
Figure 23. - BostoMatic vs. Zeiss - Standard Sphere Range Difference .....	45
Figure 24. - Plot of 3.745 Inch Linear Dimension.....	49
Figure 25. - Plot of -0.500 Inch Linear Dimension.....	49
Figure 26. - Probe Pretravel Variation at 0° and 90° vs. Approach Angle.....	53
Figure 27. - AVS/Express Force Visualization on Phase Two Artifact .....	60
Figure 28. - Vision for Future OMA Development .....	65
Table 1. - OMA and Conventional Acceptance Time Requirements ....	24
Table 2. - Coefficients for Second Through Fourth Degree Polynomials .....	31
Table 3. - P-Values for Points #1 - #145 .....	34
Table 4. - Average Values and Differences - BostoMatic vs. Zeiss in Point #1 (mm) .....	35
Table 5. -. Worst Case BostoMatic Artifact Range and Sigma (mm) .....	41

Table 6. - Worst Case BostoMatic Standard Sphere Range and Sigma (mm) .....	41
Table 7. - Standard Deviations - Benchmark CMM Data (inch) .....	50
Table 8. - Range - Benchmark OMI Data (Inch) .....	50
Table 9. - t-test and F-test of Benchmark CMM and OMI Data (inch) ....	52
Table 10. - t-test and F-test of Benchmark CMM and Corrected OMI Data (inch).....	52
Table 11. - Differences at 0° and 90° - Probe Pretravel Variation .....	53
Table 12. - Root Sum Squares of Differences at 0° and 90° - Probe Pretravel Variation.....	54
Table 13. - Comparison of Standard Deviations in Benchmark and Corrected CMM Data (inch).....	55
Table 14. - Comparison of Ranges in Benchmark and Corrected Data (inch) .....	56
Table 15. - t-test and F-test of CMM and Corrected OMI Data (inch) .....	57
Table 16. - Comparison of t-test and F-test in Benchmark and Corrected OMI Data (Inch).....	58

## 15.0 References

1. SAND95-3061, "Laboratory Directed Research and Development - Interim Report - Intelligent Tools for On-Machine Acceptance of Precision Machined Components", N. G. Christensen, L. D. Harwell, M. L. Abate
2. "Status of On-Machine Acceptance Systems and Methodologies in Small Lot, High Precision Machining Applications", Markowitz and McNaughton, Inc.
3. SAND96-8237, "Bibliography of Papers, Reports, and Presentations Related to Point-Sample Dimensional Measurement Methods for Machined Part Evaluation", J. M. Baldwin
4. Report, from Don Sheaffer, 8120, to Naomi Christensen, 2645, subject: "On-Machine Acceptance Visualization"
5. SAND96-2631, "Laboratory Directed Research and Development - Intelligent Tools for On-Machine Acceptance of Precision Machined Components - Data Sets", N. G. Christensen, L. D. Harwell, A. Hazelton
6. SAND95-2981, "Performance Evaluation of the BostoMatic 300 Machining Center", A. E. Bryce, D. E. Clingan, N. G. Christensen, L. D. Harwell
7. Memo: dated July 31, 1996, from Mark Powell, 9611, to Naomi Christensen, 2645, subject: "Error Mapping of the BostoMatic 300 for the On-Machine Inspection LDRD"

8. Memo: dated September 8, 1996, from Marcey Abate, 12323, to Naomi Christensen, 2645, subject: "Summary of LDRD Findings"

Intelligent Tools for On-Machine Acceptance of Precision Machined Components

Distribution:

Allied Signal Kansas City Division

P. O. Box 419159

Kansas City, MO 64141-159

1	C. Thompson, Jr., Dept. 010	1	J. N. Vance, Dept. ME1-1
1	K. Thomas, Dept. A21	1	J. Dycus Dept. ME1-4
1	J. Richardson, Dept. 400	1	J. Eiman, Dept. ME1-4
1	J. Jeffries, Dept. 400	1	M. S. King, Dept. ME1-4
1	M. G. Clinesmith, Dept. 427	1	L. K. Gillespie, Dept. ME1-5
1	MS0960 J. Q. Searcy, 1400	1	MS0311 J. W. Hole, 2671
5	MS0958 J. W. Munford, 1484	1	MS0328 J. A. Wilder, 2674
5	MS0958 L. D. Harwell, 1484	1	MS0328 M. J. Stevenson, 2674
1	MS0863 D. A. Pfeiffer, 1484	1	MS0188 C. E. Meyers, 4523
1	MS0958 E. A. Bryce, 1484	1	MS0188 D. L. Chavez, 4523
1	MS0958 D. E. Clingan, 1484	1	MS0980 L. J. Krumel, 5725
1	MS0953 W. E. Alzheimer, 1500	1	MS0722 J. L. Mitchiner, 6614
1	MS0665 L. J. Azevedo, 1541	1	MS9401 D. A. Sheaffer, 8120
1	MS0665 J. Chamberlin, 1541	1	MS9420 L. A. West, 8200
1	MS1453 F. H. Braaten, 1553	1	MS9430 L. N. Tallerico, 8204
1	MS1453 T. M. Witt, 1553	1	MS9420 J. M. O'Connor, 8220
1	MS0516 G. L. Laughlin, 1564	5	MS9430 A. J. West, 8240
1	MS0521 T. J. Young, 1567	1	MS9430 C. A. Steinhaus, 8240
1	MS0342 K. W. Mahin, 1807	1	MS9007 R. C. Wayne, 8400
1	MS9405 D. L. Lindner, 1809	1	MS9105 D. M. Kwon, 8412
1	MS0457 H. W. Schmitt, 2000	1	MS1002 P. J. Eicker, 9600
1	MS0447 J. O. Harrison, 2111	1	MS1003 R. W. Harrigan, 9602
1	MS0447 R. E. Kreuzfeld, 2111	1	MS1003 R. D. Robinette, 9611
1	MS0503 R. B. Diegle, 2338	1	MS1010 M. E. Olson, 9622
1	MS0985 J. H. Stichman, 2600	1	MS1006 P. Garcia, 9671
1	MS0985 D. H. Schroeder, 2605	1	MS9037 R. E. Stoltz, 12120
1	MS0329 D. W. Plummer, 2643	1	MS0631 W. C. Nickell, 12300
1	MS0329 M. J. Craig, 2643	1	MS0829 K. V. Diegert, 12323
10	MS0319 W. R. Leuenberger, 2645	1	MS0829 M. L. Abate, 12323
1	MS0319 P. J. Skogmo, 2645	1	MS1068 G. N Beeler, 14000
50	MS0319 N. G. Christensen, 2645	1	MS0856 M. E. Sheldon, 14308
1	MS9018 Central Technical Files, 8940-2		
5	MS0899 Technical Library, 4414		
3	MS0161 Patent and Licensing Office, 11500		
2	MS0619 Review and Approval Desk, 12690 for DOE/OSTI		